TD-10-012

Fermilab

Fermi National Accelerator Laboratory
Technical Division
SRF Development Department
P.O. Box 500
Batavia, IL 60510
Fax: (630) 840-8036

Design of a Probe for Strain Sensitivity Studies of Critical Current Densities in SC Wires and Tapes

N. Dhanaraj, E. Barzi, D. Turrioni, A. Rusy, V. Lombardo

Table of Contents

S. No	Title	Page No.
	Abstract ……..	1
1.0	Introduction ……	3
2.0	Spring Design …….	3
	2.1 Theory ……	3
	2.2 Design Constraints……	4
	2.3 Shape Optimization ……	5
	2.4 Analytical Model ……	7
	2.5 Finite Element Model……	8
3.0	Design of the Probe…….	13
	3.1 Strain Application Procedure……	14
	3.2 Strain Measurement ……	16
	3.3 Probe Assembly ……	18
4.0	Resistance Calculations ……..	19
	4.1 Contact Resistance ……	19
	4.2 Splice Resistance ……	22
5.0	Current Lead Optimization ……	24
	5.1 Thermal Model ……	24
	5.2 Lock's Optimization ……	26
	5.3 LEADX Simulation ……	29
6.0	Structural Analysis …….	30
	6.1 Torsion of Outer Tube ……	30
	6.2 Shear Stresses in Pins/Bolts ……	32
7.0	Summary ……	32

List of Figures

Figure 1	Schematic of loading of the spring section ……	3
Figure 2	Schematic of the spring cross section with the dimensions……	6
Figure 3	Segment of spring showing the moment directions ……...	7

Figure 4	(a) 3D Model of the spring (b) Section view of the spring ….....	8
Figure 5	Finite element model of the helical spring showing the loading scheme ……...…….	9
Figure 6	Circumferential strain for angular displacements of 10°, 20° and 70°……	10
Figure 7	Von-mises stress of Ti-6Al-4V spring at 70° angular displacement ……...	11
Figure 8	Von-mises stress of CuBe spring at 70° angular displacement .	12
Figure 9	Schematic of the probe setup……..	14
Figure 10	3D model of inner tube assembly ……..	15
Figure 11	(a) Gear box assembly (b) Vacuum chamber around the gear box ……..	16
Figure 12	Setup to measure the angular displacement of the spring ……..	17
Figure 13	Full assembly of the probe …….	19
Figure 14	Interfaces contributing to resistance of current flow …….	21
Figure 15	Image showing the splice interface regions ……...	23
Figure 16	Model for the estimation of joint resistance ……...	23
Figure 17	Schematic model of an elemental length of lead showing the direction of heat flow …….	27
Figure 18	Result from Lock's analysis showing relationship between lead geometry and residual resistivity…….	28
Figure 19	Temperature profile in the lead for a warm end temperature of 300 K using LEADX simulation ……	30
Figure 20	Plot of von-mises stresses in the outer current tube……	31

List of Tables

Table 1	Material properties of Ti-6Al-4V and Beryllium Copper……...	9
Table 2	Angular displacements and corresponding circumferential strains: analytical and FEA……...…….	13
Table 3	Geometry of current leads ……..	29
	References……	37

Appendices

Appendix 1	Optimization procedure for helical spring cross section…….	39

Appendix 2	Analytical solution for torsion of helical spring with T-shaped cross section…… ……...	44
Appendix 3	Resistance calculations ……..	46
Appendix 4	Optimization of current leads – J. M. Lock's method ……...	52
Appendix 5	Shear stress calculations……..	58

Abstract

The design of a variable-temperature probe used to perform strain sensitivity measurements on LTS wires and HTS wires and tapes is described. The measurements are intended to be performed at liquid helium temperatures (4.2 K). The wire or tape to be measured is wound and soldered on to a helical spring device, which is fixed at one end and subjected to a torque at the free end. The design goal is to be able to achieve ± 0.8 % strain in the wire and tape. The probe is designed to carry a current of 2000A.

1.0 Introduction

The critical current density (J_c) of superconducting wires and tapes used in magnets is highly sensitive to axial strain and hence an accurate measurement of this strain dependence is critical for the proper design and application of high field magnets. Considerable effort has been dedicated in the past to these strain sensitivity studies and the greatest challenge has been obtaining a reliable and accurate measurement that calls for long samples in order to have considerable distance between the voltage taps whilst being limited in space by the size of the magnet bore. Many methods and techniques have been adapted and in general the studies fall into one of the two categories: monotonic axial loading technique or bending spring technique as claimed by Taylor et al. [1]. The axial loading technique is simpler and straight-forward and is very similar in principle to a tensile test measurement wherein a short sample is loaded axially by gripping and pulling at the ends. The grips also serve as the current leads measuring the critical current density as a function of axial strain. The main disadvantage of this technique is the length of the sample; which is usually short (~ 40 mm) [1] and hence the distance between the voltage taps are not sufficient for reliable and accurate measurements and consequently limiting the sensitivity of measurements [1]. Also, the axial loading technique typically allows only tensile measurements to be performed. The bending spring on the other hand helps overcome the constraint in the directionality of measurement and allows both tensile and compressive strains to be applied on the sample. The U-spring [2-4], Pacman [5] and Walters's spring [1, 6-8] are some of the devices which use the concept of bending of a curved beam on which the sample is mounted. The U-spring has sample lengths approximately equal to the size of the magnet bores and the Pacman samples are

approximately the circumference of the bore (max length ~120 mm). The Walters' spring device, originally proposed by C.R. Walters' et al., is a helical spring with either a T-shaped or rectangular cross section. The spring is fixed at one end and subjected to a torque at the free end which induces circumferential strain in the wire or tape mounted on the outside of the spring. The Walters's spring can handle long samples ~ 800 mm [1, 6, 7, 11], thus enabling reliable measurements to be performed. However, the spring also poses some constraints due to the material properties. In order to perform accurate high strain measurements the spring material needs to remain elastic in the measuring regime and thus a material which is highly elastic at high strains and low temperatures (4.2 K) is required. The material used for these springs are usually Ti-6Al-4V and CuBe (Beryllium Copper). The Ti-6Al-4V material exhibits higher elasticity ~ 1.3 % [1, 6, 8] compared to CuBe, but has poor solderability and thus requires some plating [1, 6, 9] prior to attaching the sample. CuBe does not pose problems for soldering but has lower elasticity 0.7 to 0.8 % [7-8]. The soldering of the sample to the Walters's spring device also induces thermal strains due to the difference in the co-efficient of thermal contraction in the different materials. As measured by [1] this causes only an additional strain to the intrinsic strain of the spring and hence can be accounted for. Also, the spring exhibits strain gradients across the cross section and along the length the effects of which can be minimized by optimizing the shape of the cross section and size of the spring. From the above literature review and investigation into a reliable strain measuring device we have designed a helical spring based on the methodology described by Walters's and adapted by Taylor et al. The spring device described here has a T-shaped cross section and is capable of handling both wire geometry and tape geometry. The choice and design of this spring device also allows us to use our existing setup used for variable temperature studies of wires and tapes. The probe is essentially made of two concentric OFHC copper tubes which act as current and torque (load) carriers. The sample to be measured is mounted on the spring; the bottom of the spring is fixed and attached to the outer current tube which carries the current to the sample. The top of the spring is attached to the inner tube which carries the current from the sample. The torque is generated via a manual worm-gear setup that can handle a max. torque ~ 60 N.m. and transmitted to the sample through the inner tube and spring assembly. The top of the outer tube is bolted on to the

dewar and hence is not free to rotate. The design discussed in this paper utilizes the major parts of the existing probe and thus enabling reliable cost efficient studies. The measurements will be performed on both Ti-6Al-4V and CuBe spring materials.

2.0 Spring Design

2.1 Theory:

The working principle of the spring is similar to the bending of a curved beam. The spring can be described as a beam with a given cross-section wound on a cylinder with a specific pitch to obtain a helical pattern and thus each turn of the spring represents a curved section of the beam [6] as shown in the schematic figure 1. The torque applied at the end of the spring depending on its direction induces circumferential tensile strain on the outer radius of the spring above the neutral axis of the section and circumferential compressive strains below the neutral axis, the strain states are reversed with the direction of the torque. The strains can be analytically computed for a given section using the formula for strains in a curved beam.

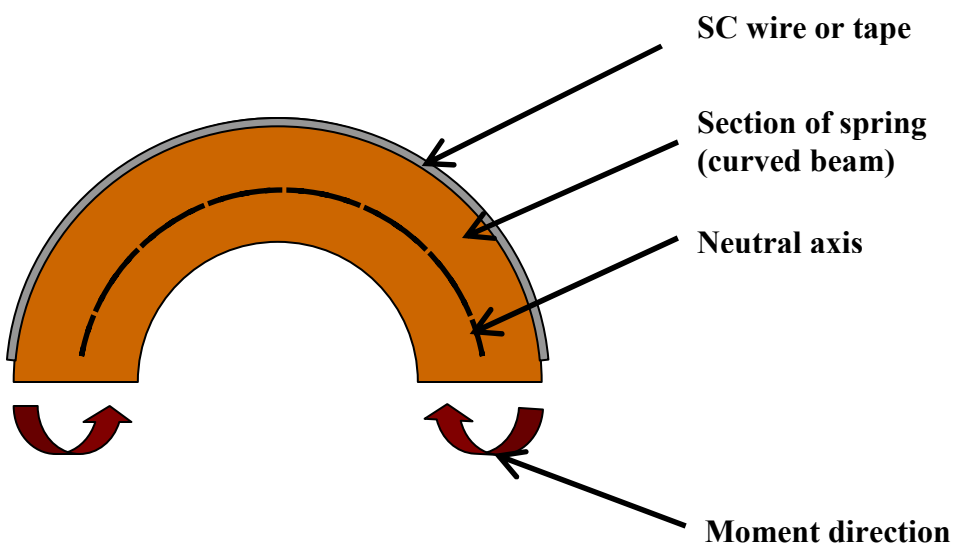

Figure 1. Schematic of loading of the spring section

As described in [6] the circumferential strain $\varepsilon_{\theta\theta}$ in a helical bending spring as a function of the radial distance r is given as:

$$\varepsilon_{\theta\theta} = K(1 - r_n / r) \tag{1}$$

where K is a factor that depends on applied angular displacement θ , the number of turns of the spring N and the pitch angle α:

$$K = (\theta / 2 \pi N) \cos \alpha \quad (2)$$

The location of the neutral r_n can be calculated by using the condition that the net force perpendicular to the cross-section of the spring is zero [6]:

$$\int w(r)E(r)\varepsilon_{\theta\theta}(r)dr = 0 \quad (3)$$

where w is the width of the cross-section along the longitudinal axis of the spring which varies along the radius and E is the young's modulus as a function of radius to account for spring material and wire material. Equation (3) can be solved analytically to locate the neutral axis and used in conjunction with eqn. (1) to obtain the strain in the section of the spring.

2.2 Design Constraints:

The first step towards designing the spring was to address the constraints imposed by our existing system and the performance goals. The two main types of spring cross sections under study [1, 6-7] have been rectangular and T-shape. Typically, the rectangular spring has been used for tapes and the T-shape for wires. Studies [6] have shown that the T-shape springs have greater torsional rigidity compared to the rectangular cross section and also the sinusoidal strain variations along the length of the sample is smaller in the T-shape. Also, a spring with an integer number of turns exhibits smaller strain oscillations and as the number of turns increase the spring becomes less rigid and its ability to withstand higher strains decreases. Thus a T-shape cross section with 4 turns was chosen as the design baseline. The outside diameter of the spring was constrained by the size of the current carrying tubes and the bore size. As the spring is attached to the inner tube which is concentrically placed within the outer tube, the inner diameter 1.62" of the outer tube was the limit. Accounting for minimal clearance for helium flow and the voltage tap wires, the outside diameter of the spring was chosen to be 1.25".

2.3 Shape Optimization:

The design and optimization of the spring cross section is critical to the design of the spring as it dictates the strain values to which the spring can be subjected, determines the corresponding angular displacement and the torque required to achieve it. An optimal cross section minimizes the ratio of the strain at the inner surface of the spring to the strain at the outer surface of the spring and also reduces the strain gradient across the wire or tape to be measured. The optimization procedure described here was originally proposed by Walters' [6] and later adapted by Taylor et al. [1], the detailed calculations are shown in appendix 1. The steps involved are as follows:

a) Maximize the outer diameter of the spring depending on the space available in the cryostat. In our case as mentioned in the design constraints the outer diameter of the spring was limited to 1.25" or 31.75 mm.
b) Maximize the width (w2) at the inside of the section by choosing an appropriate pitch which is about ¼ of the outer diameter of the spring. The width at the inside is then ~ 0.8 * (pitch). In our case the pitch is 8 mm and the width is 7 mm.
c) Minimize the width (w1) at the outside of the spring. For wires a width of about twice the diameter is chosen, here we chose a width of 5.5 mm to accommodate both 1 mm diameter wires and ~ 4.7 mm wide tapes.
d) Assume a value for the inner radius (r2) and find the step position, i.e. where the 45° chamfer begins, such as to minimize the neutral radius and the strain ratio. This is done by choosing discrete values of r2 and the step position and calculating the neutral radius using eqn. (3) and the strains from eqn. (1).

The procedure allows us to approximately determine the angular displacement of the spring for a given strain ratio and also gives the strain values at the inside and outside of the spring. In our design, the strain ratio is slightly greater than 1 (1.133) and thus the strain at the inside is slightly higher than the strain at the outside, although we are still able to achieve the design goal of ± 0.8 % strain at the outside. The strains here do not take into account the thermal contraction that would occur during measurements at 4.2 K. The cross section of the spring is shown in figure 2.

The torque required to achieve a certain strain at the outside of the spring can be calculated from the equations of stresses in a curved beam subjected to bending. In our design the strain at the outside is required to be ± 0.8 % and thus the torque is given by:

$$T = \frac{\sigma_o . A.e.r_o}{C_o} \tag{4}$$

Where σ_o is the stress which is a product of the strain and the young's modulus (E) of the material,

A is the area of the cross section in mm^2,

$e = r_c - r_n$, is the eccentricity in mm, r_c is the centroid, r_n is the neutral radius,

$C_o = r_o - r_n$, distance from neutral axis to outer surface in mm, r_o is the outer radius.

The detailed torque calculations are shown in appendix 1.

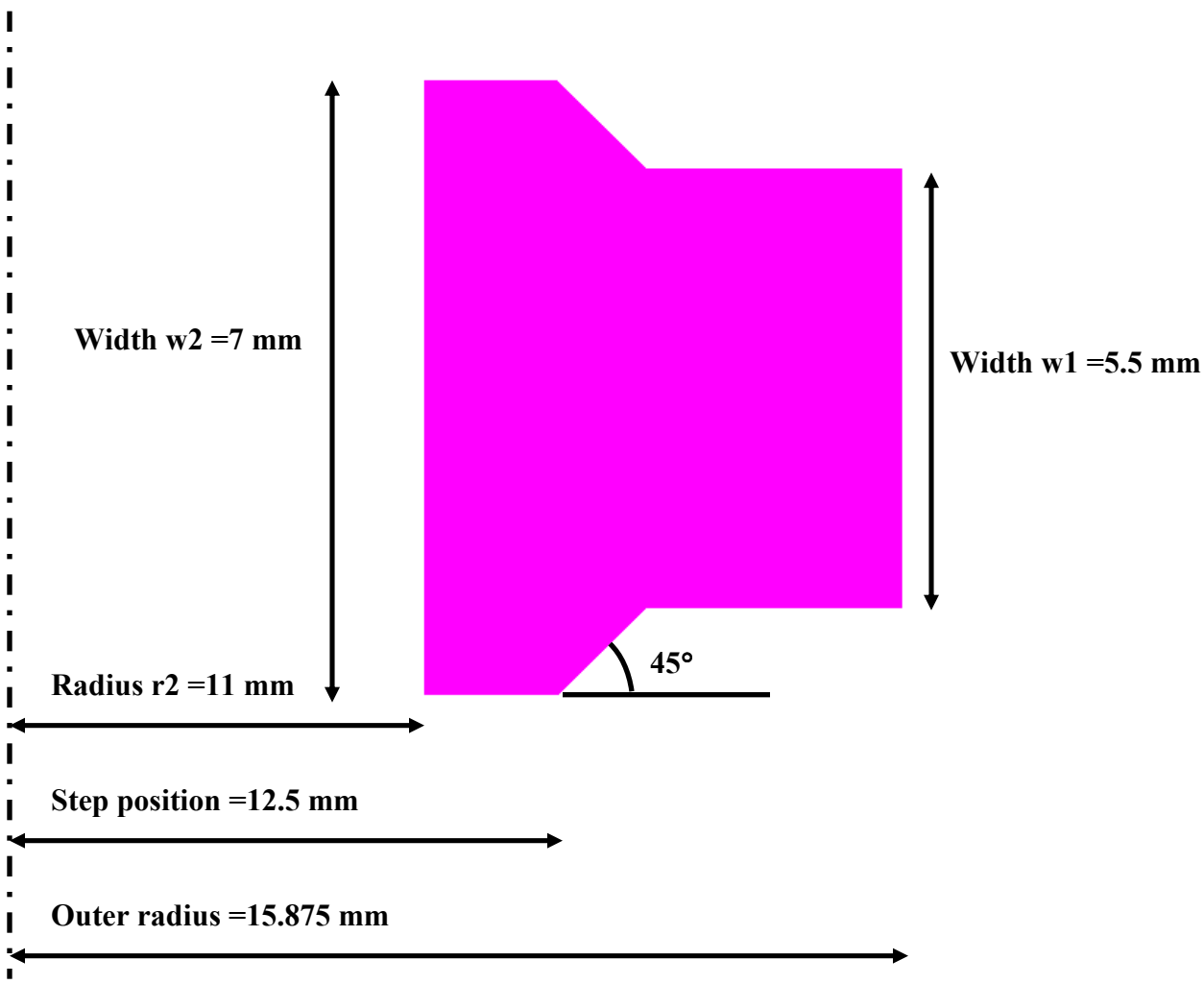

Figure 2 Schematic of the spring cross section with the dimensions

2.4 Analytical Model:

The problem of a helical spring fixed at one end and subjected to a torque or twisting moment at the other end can be solved analytically as described in [10]. This approach helps to determine the rotation of the spring about its vertical axis, i.e. angular displacement of the free end with respect to the fixed end, the twisting of the spring segment about the axis of the spring wire and also the change in length that occurs as the spring is twisted for a given torque value. The solution is more accurate for springs of circular cross section and for springs of non-circular cross sections an approximate solution can be obtained by the following the assumptions described in [10]. The detailed calculations are shown in appendix 2. Figure 3 gives the schematic of the loading of a segment of the spring, .i.e. the torque applied and its components.

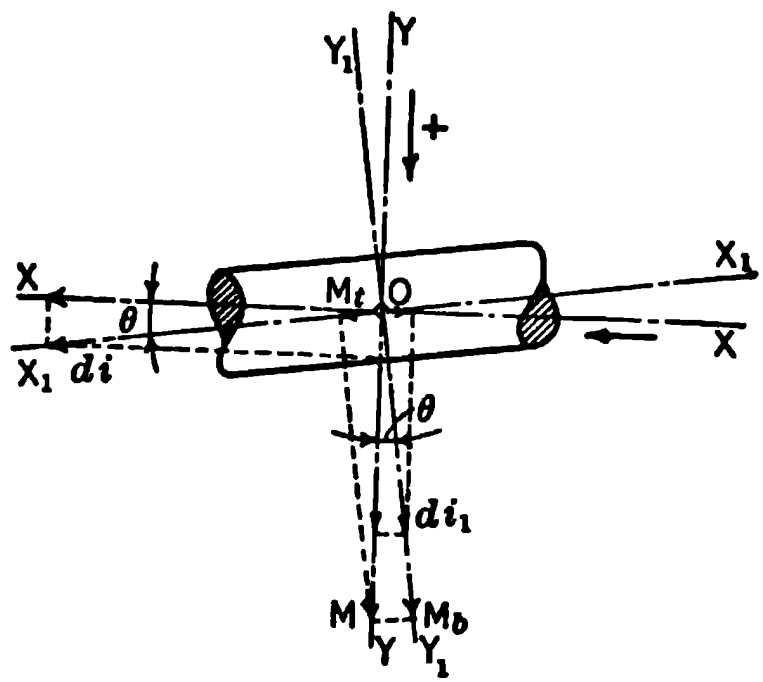

Figure 3. Segment of spring showing the moment directions [10].

The total rotation of the free end of the spring about axis OY can be obtained by analyzing the segment shown above and is given by:

$$\phi = l\left(\frac{M_t Sin\theta}{GI_p} + \frac{M_b Cos\theta}{EI}\right) \tag{4}$$

The total rotation about the axis OX is given by:

$$\omega = l\left(\frac{M_t Cos\theta}{GI_p} - \frac{M_b Sin\theta}{EI}\right) \tag{5}$$

and hence the total change in length of the spring is given by:

$$\delta = \frac{D}{2}\omega \tag{6}$$

where the length of the coil is given as, $l = n\pi D \sec\theta$ (7)

The torque M is resolved into components

$M_b = MCos\theta$ and $M_t = MSin\theta$, i.e. bending and twisting components.

G =0.4 E, which is the young's modulus of the material.

I and I_p are the area and polar moment of inertia of the cross section and θ is the helix angle of the spring and D the diameter of the coil.

The angular displacement for a given torque value obtained here is comparable to that determined in the optimization procedure. Also, the extra information on the total change in length can also be obtained from this analytical solution which is critical for the design of the spring and the probe. The total length of the spring has been designed to be 64.25 mm to accommodate the 4 turns (as shown in fig. 4) and also to be able to position the spring across the magnetic center line in the cryostat during the test.

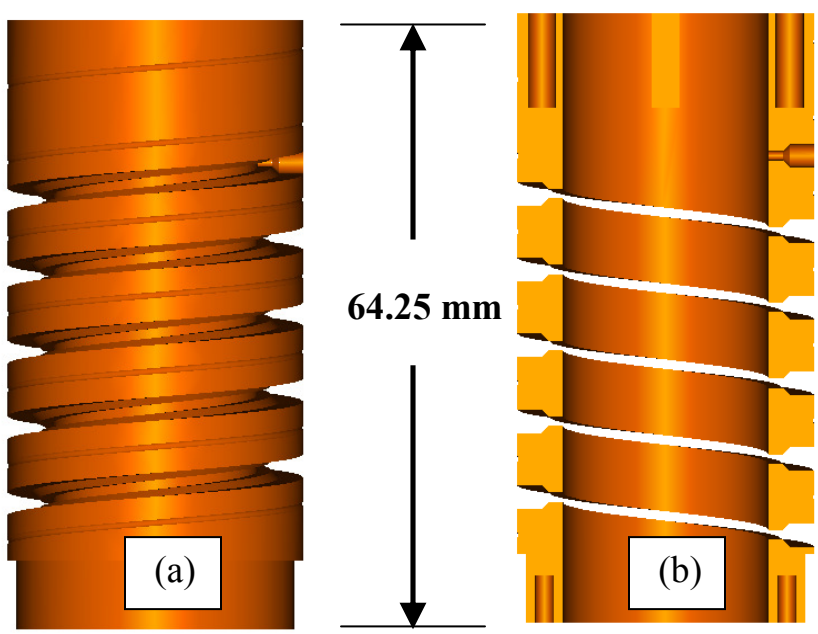

Figure 4. (a) 3D Model of the spring (b) Section view of the spring

2.5 Finite Element Model:

A finite element model of the spring was developed to verify the analytical solution and also to better understand the complexities involved when the spring is subjected to torque loading at cryogenic temperatures. The analysis was performed on a 3D model of the 4 turns of the spring, shown in fig 5 using the commercial software ANSYS. The model was meshed with 15665 solid brick elements and the load was applied by constraining the bottom face of the spring and applying an angular displacement at the top face of the spring. The analysis was performed for two different spring materials, Ti-6Al-4V and Beryllium Copper (alloy 25), the material properties of which are shown in table 1.

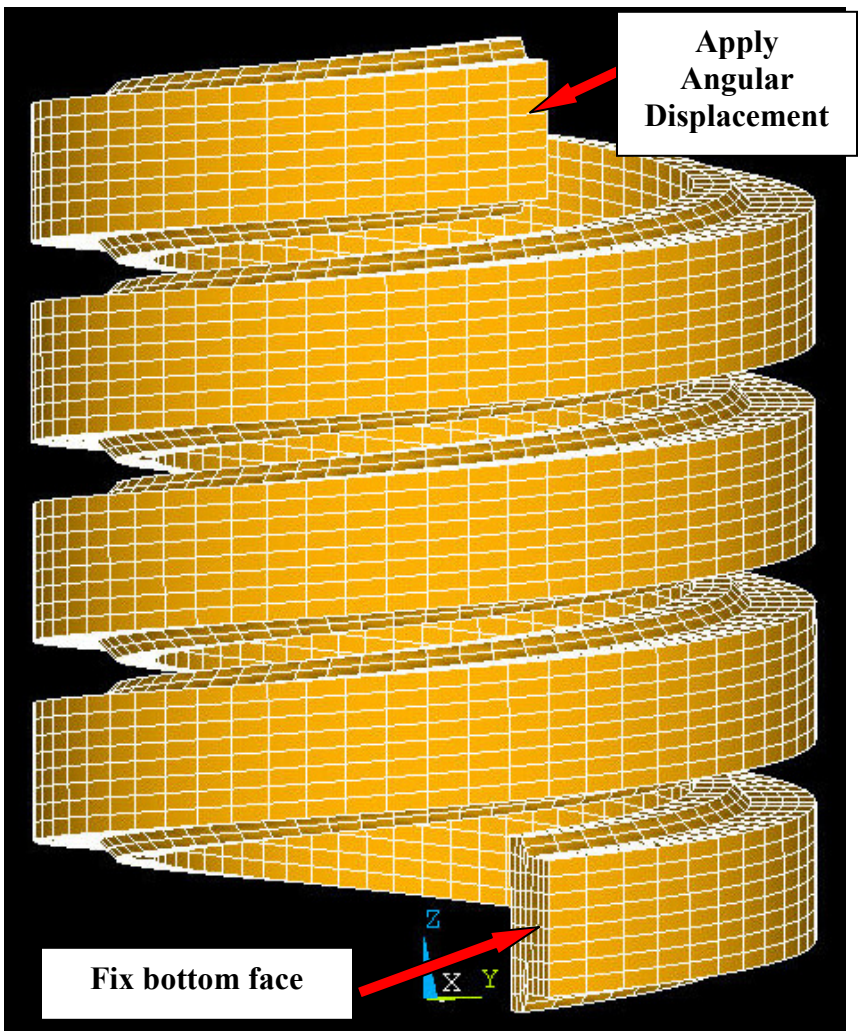

Figure 5 Finite element model of the helical spring showing the loading scheme

Property	Ti-6Al-4V		Beryllium Copper (alloy 25)	
	293 K	**4.2 K**	**293 K**	**4.2 K**
Young's Modulus (GPa)	110	130	117.9	132.4
Yield Strength (MPa)	904.6	1710	1189.65	1390.5
Tensile Strength (MPa)	965.3	1771	1366.81	1526.5

Table 1. Material properties of Ti-6Al-4V and Beryllium Copper [12, 13].

The analysis was carried out in 2 load steps; the first step involves a cool down of the spring from 293 K to 4.2 K, the strain due to thermal contraction was found to be small in the order of 1e-9 to 1e-7 and hence can be ignored for practical purposes. However, in reality the sample will experience some thermal strain during the cool down as it would be soldered on the spring which can be deduced by attaching strain gages on the sample as a part of initial calibration studies. Nevertheless, it has been shown that these thermal strains do not alter the strain state of the spring [1].

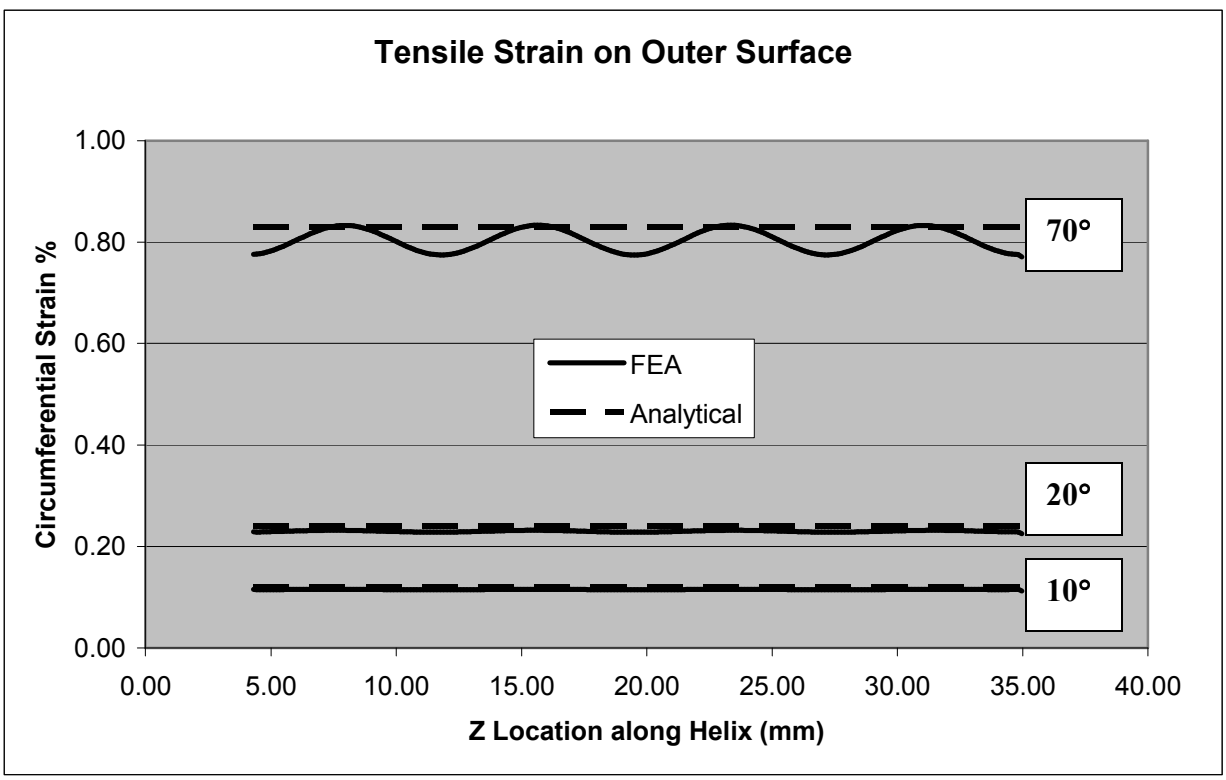

Figure 6. Circumferential strain for angular displacements of 10°, 20° and 70°

In the second load step, an angular displacement was applied to the top face of the spring to induce tensile or compressive stresses at the outer face of the spring. The

simulation uses the nonlinear solution approximation due to the large deflections involved. Figure 6 shows the plot of the circumferential strain for given angular displacements applied in the counter clockwise direction inducing tensile strains at the outer face. The strains are measured along the mid line of the outer face where the wire would contact the spring.

The strains exhibit a sinusoidal variation along the helical path, the magnitude of which increases with the applied angular displacements. Studies [1] have shown that these oscillations occur due to the twisting of the spring segments along their self-axes when subjected to torsion and can be minimized by choosing a rigid cross section, such as a T-shaped section and also with integer number of turns. Ideally, the circumferential strain is independent of the material of the spring although in reality some variation should be expected due to the difference in the thermal expansion coefficient of materials.

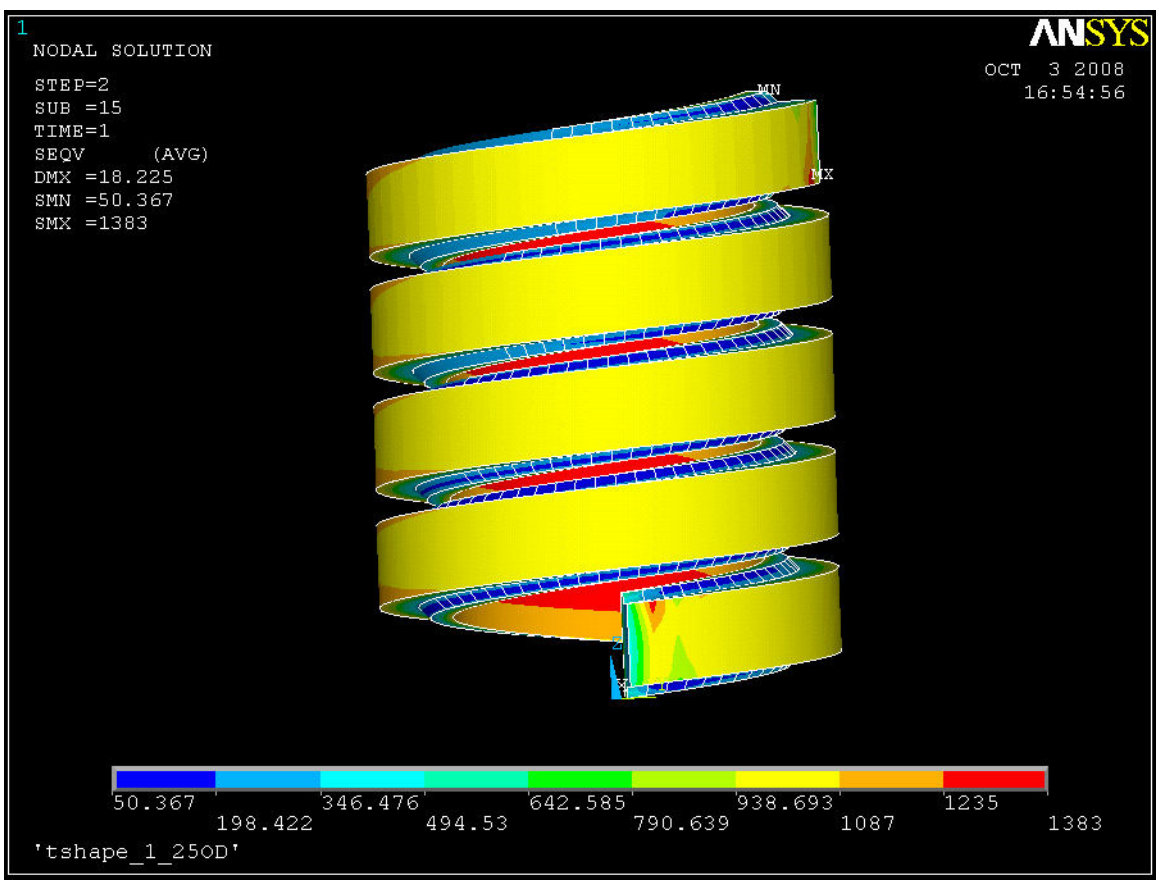

Figure 7. Von-mises stress of Ti-6Al-4V spring at 70° angular displacement

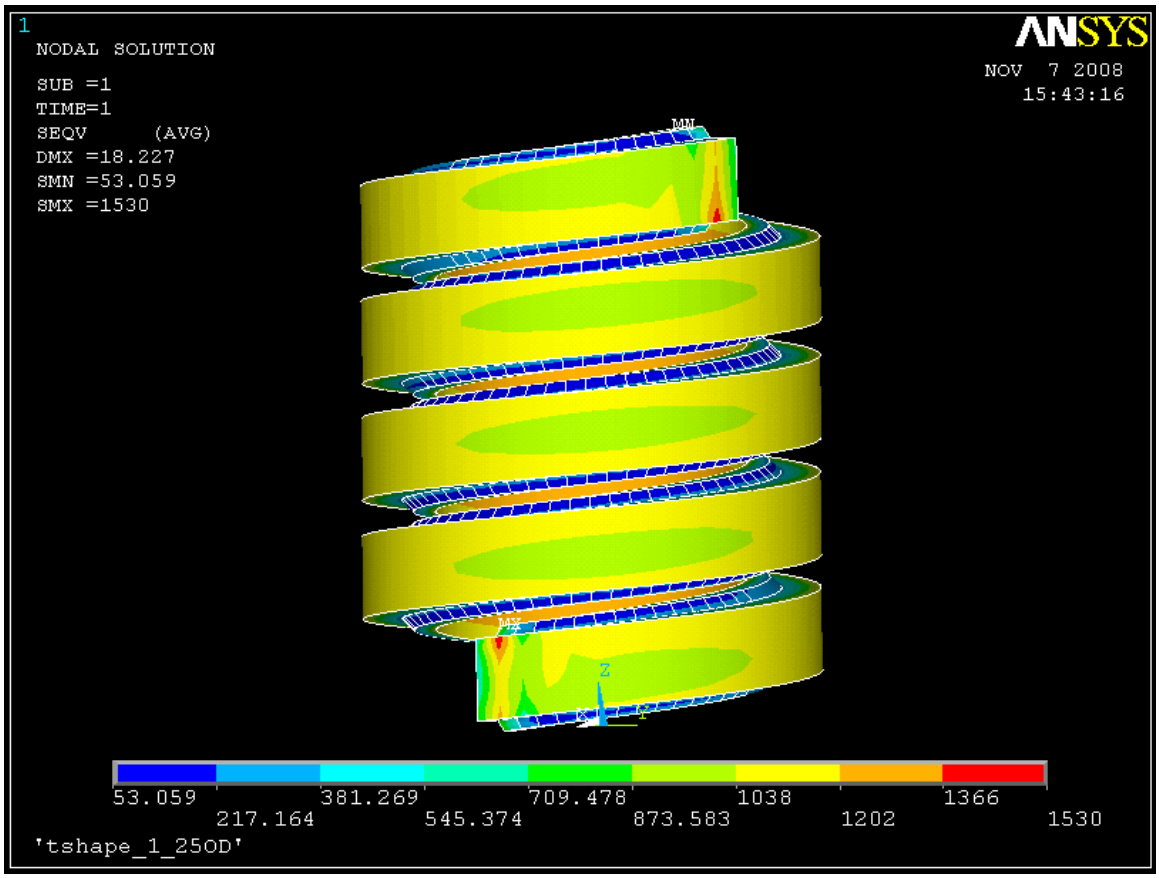

Figure 8. Von-mises stress of CuBe spring at 70° angular displacement

Figures 7 and 8 show the von-mises stresses in the Ti-6Al-4V and Beryllium Copper (CuBe) spring for an applied angular displacement of 70° ccw which induces 0.8 % tensile strain at the outer surface of the spring. The Ti-6Al-4V spring is able to withstand the strain without any yielding although the CuBe spring experiences some yielding and in order to operate in the elastic regime, the loading should be reduced. The CuBe spring can withstand ~ 0.75% strain without yielding. Table 2 shows the loading chart and the correlation between applied angular displacement and circumferential strain.

The FEA was used to verify few cases and in general the spring experiences 0.012 % of circumferential strain per degree of rotation. The FEA results (strains) are in good agreement with the analytical solution for small angular rotation and the variation in about 4% for the max. angular rotation of 70°. The analytical solution is based on pure bending of a curved beam and does not take into account the lateral compression; a strain

gage calibration will help determine the strains experienced by the sample more accurately.

Angular Displacement (Degrees)	**Circumferential Strain at Outer Surface of Spring (%)**	
	Analytical $\varepsilon_{\theta\theta} = K(1 - r_n / r)$	**FEA (Average Strain along midline)**
0	**0.00**	
4	**0.05**	
8	**0.09**	
10	**0.12**	**0.12**
12	**0.14**	
16	**0.19**	
20	**0.24**	**0.23**
24	**0.28**	
28	**0.33**	
32	**0.38**	
36	**0.43**	
40	**0.47**	
44	**0.52**	
48	**0.57**	
52	**0.62**	
56	**0.66**	
60	**0.71**	
64	**0.76**	
68	**0.81**	
70	**0.83**	**0.81**

Table 2. Angular displacements and corresponding circumferential strains: analytical and FEA

3.0 Design of the Probe

The probe mainly constitutes an assembly of two concentric tubes; the outer tube and the inner tube, made of OFHC copper. The tubes serve as current carriers and also provide the structural basis for the transmission of torque. The outer diameter of the assembly is 1.75” (44.45 mm) and is able to handle a current of 2000 A at 4.2 K. The

schematic of the probe assembly is shown in figure 9. The strain applied to the spring is based on the methodology used by Walters' et al. and Cheggour et al.

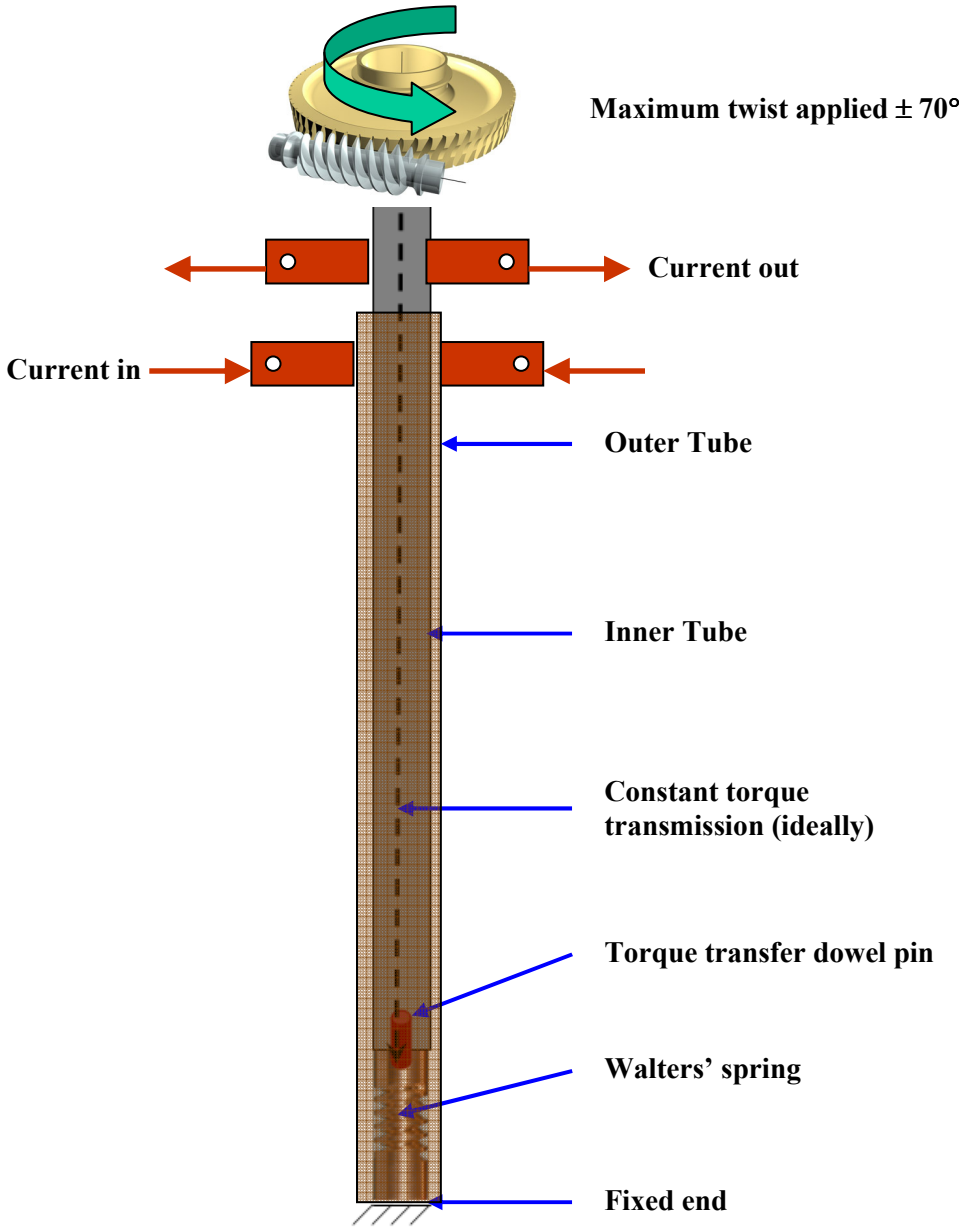

Figure 9. Schematic of the probe setup (Walters' spring shown here courtesy of NIST).

3.1 Strain Application Procedure:

The strain to be applied on the test sample originates in the form of a torque generated by a worm-gear assembly. The worm-gear pair is capable of handling a maximum torque of ~ 60 N. m. An aluminum bronze gear wheel with 50 teeth was

chosen to allow for fine torque settings. The gear wheel is mounted on top of the inner tube through dowel pins to transmit the torque. A G10 block provides electrical insulation between the tube and the gear as shown in figure 10.

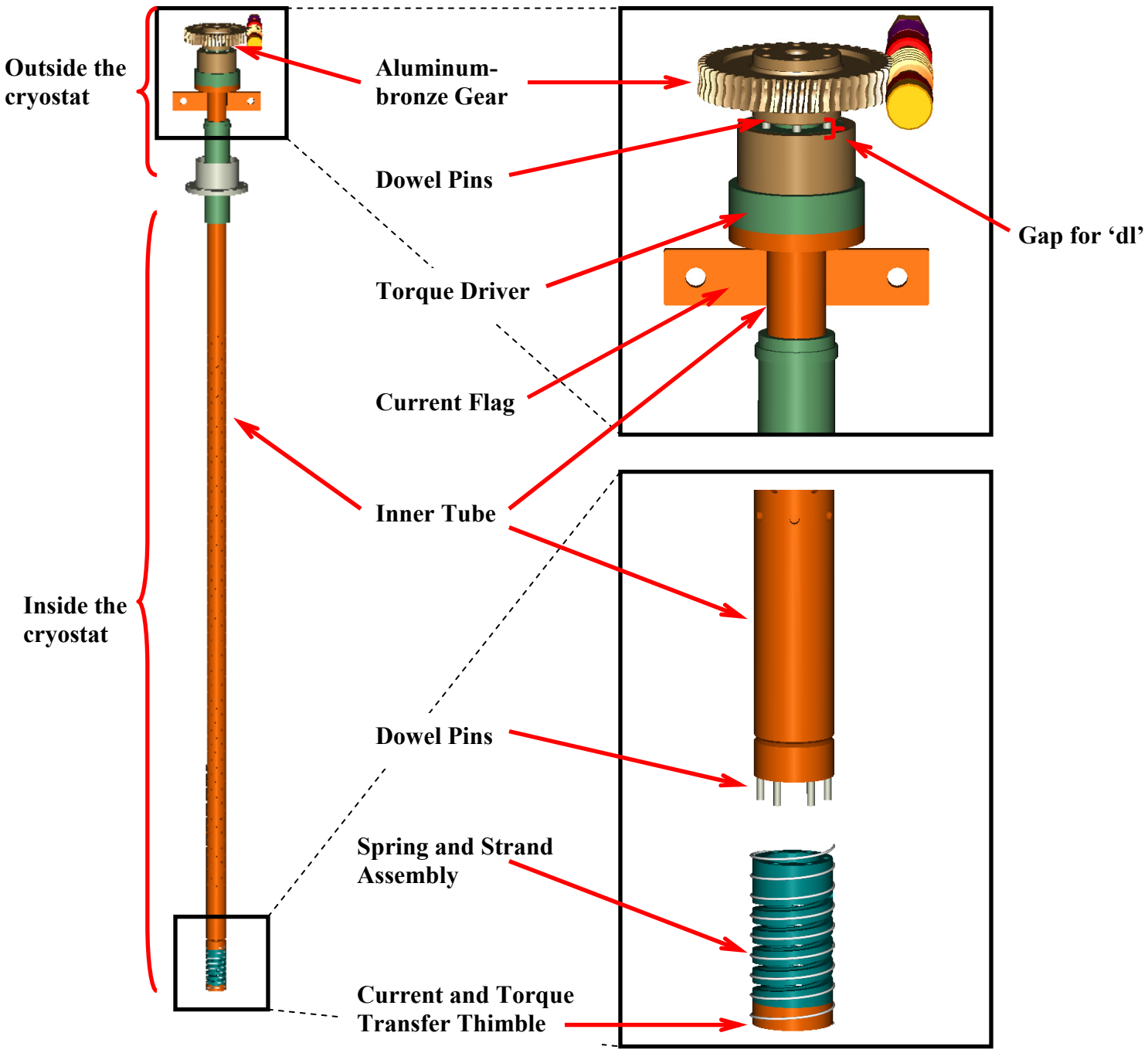

Figure 10. 3D model of inner tube assembly

Figure 10 shows the assembly in the zero torque position with a gap 'dl' between the G10 block and the gear. This gap helps accommodate the change in length experienced by the spring during strain application. The analytical solution predicts a maximum change in length of ± 1 mm, while the FEA gives a maximum of ± 0.75 mm, the design here allows a maximum of ± 4 mm. The top of the spring is connected to the inner tube through dowel pins and the bottom of the spring is bolted to a copper thimble. The thimble helps to transfer the current from the outer tube (not shown here) that envelopes the inner tube to the test sample and also helps to fix the bottom of the spring relative to its top by bolting it to the outer tube. The flex cables are connected to the current flags welded to the inner tube.

The gear set is enclosed within a gear box which is surrounded by a vacuum chamber held at a low-medium vacuum level of 1e-4 torr. This helps to protect the torque generation and transmission system from any moisture and dirt that might cause operational difficulties shown in fig. 11.

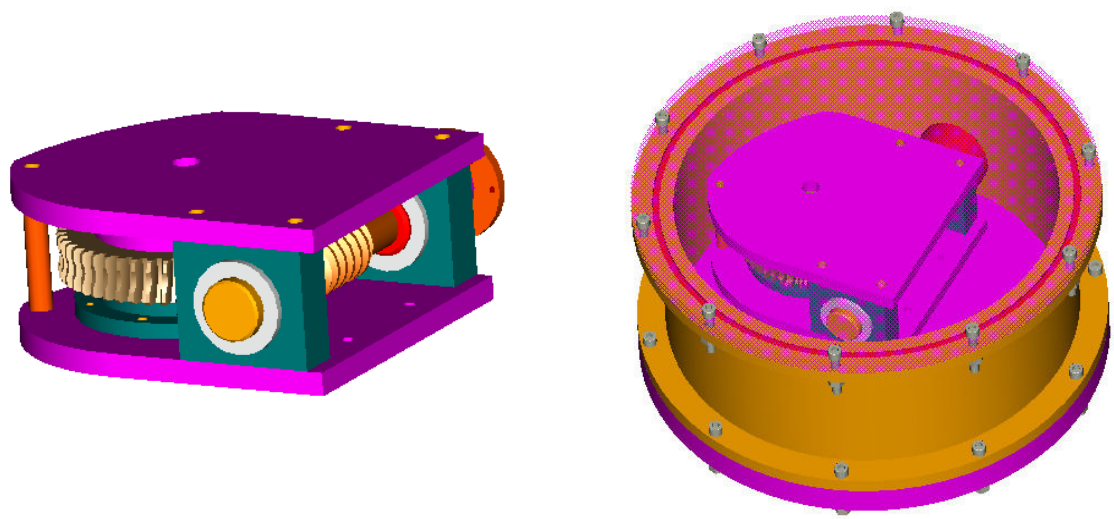

(a) (b)

Figure 11. (a) Gear box assembly (b) Vacuum chamber around the gear box

3.2 Strain Measurement:

A measurement setup (shown in fig. 12) has been designed similar to that described in [6, 7] to enable the deduction of the strain applied to the sample. The measurement assembly consists of a concentric tube and rod enclosed within the inner

tube assembly. The tube called the 'protractor shaft' has an outer diameter of 12 mm and is made of aluminum.

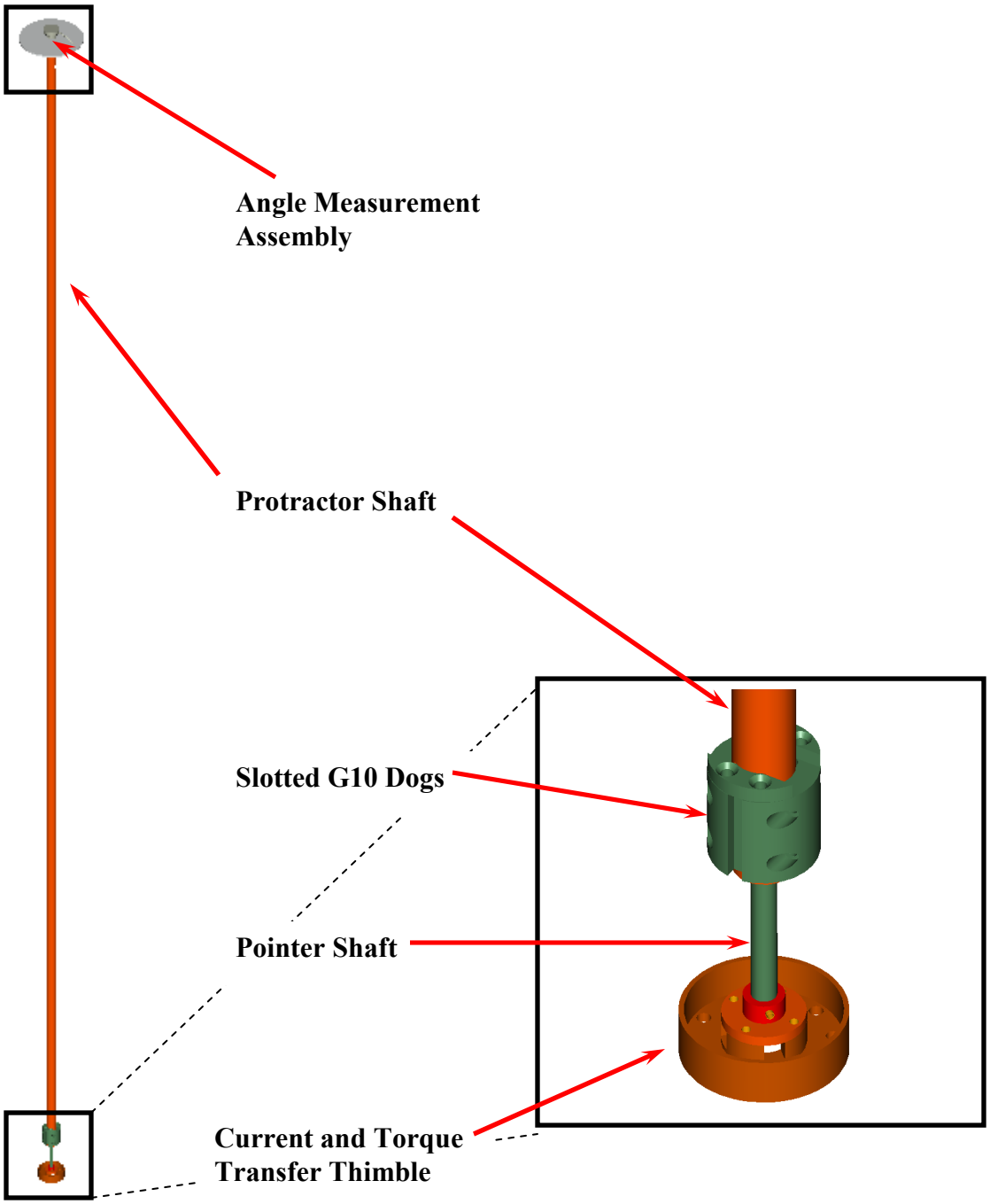

Figure 12. Setup to measure the angular displacement of the spring

A 2 piece G10 block is bolted to the bottom of the shaft and a plate with a protractor scale on it is mounted at the top of the shaft just as the shaft clears the gear box. The G10 block has slots which fit into the keys machined at the top of the spring and thus electrically insulates the shaft from the spring. Concentric and contained within the protractor shaft is a G10 rod called the 'pointer shaft'. The bottom of the pointer shaft is bolted to the copper thimble and at the top a pointer needle is pinned into it. When the torque is applied the protractor scale rotates relative to the pointer and the difference between the two gives the angular displacement of the top of the spring. The angle read from the scale can then be used to find the strain applied to the spring using the relationship described in section 2.1, equations (1) and (2).

3.3 Probe Assembly:

The strain measurement setup is contained within the inner tube and spring assembly which is enveloped by the outer tube assembly. The top of the outer tube is bolted to the top plate of the cryostat which constrains the rotation and the bottom is connected to an extension cup. The extension cup is made of OFHC copper and bolts to the outer tube at the top and to the current and torque transfer thimble and the spring at the bottom. The function of this cup is to transfer the current from the outer tube to the sample and also to transmit the torque from the spring to the outer tube.

The gear box and the vacuum chamber are supported by struts which bolt to the top plate of the cryostat. The top plate of the vacuum chamber is made of transparent polycarbonate (lexan) to aid the reading of the angular displacement. The current cables capable of handling 2000 A are connected to the outer and inner tubes via the flags welded to them. The inner tube flags can be rotated ± 77° without interference. Insulating G10 tubes with o-rings provide the necessary electrical insulation and helium seals between the outer and inner tube and also between inner and the protractor shaft. The full assembly of the probe is shown in fig. 13.

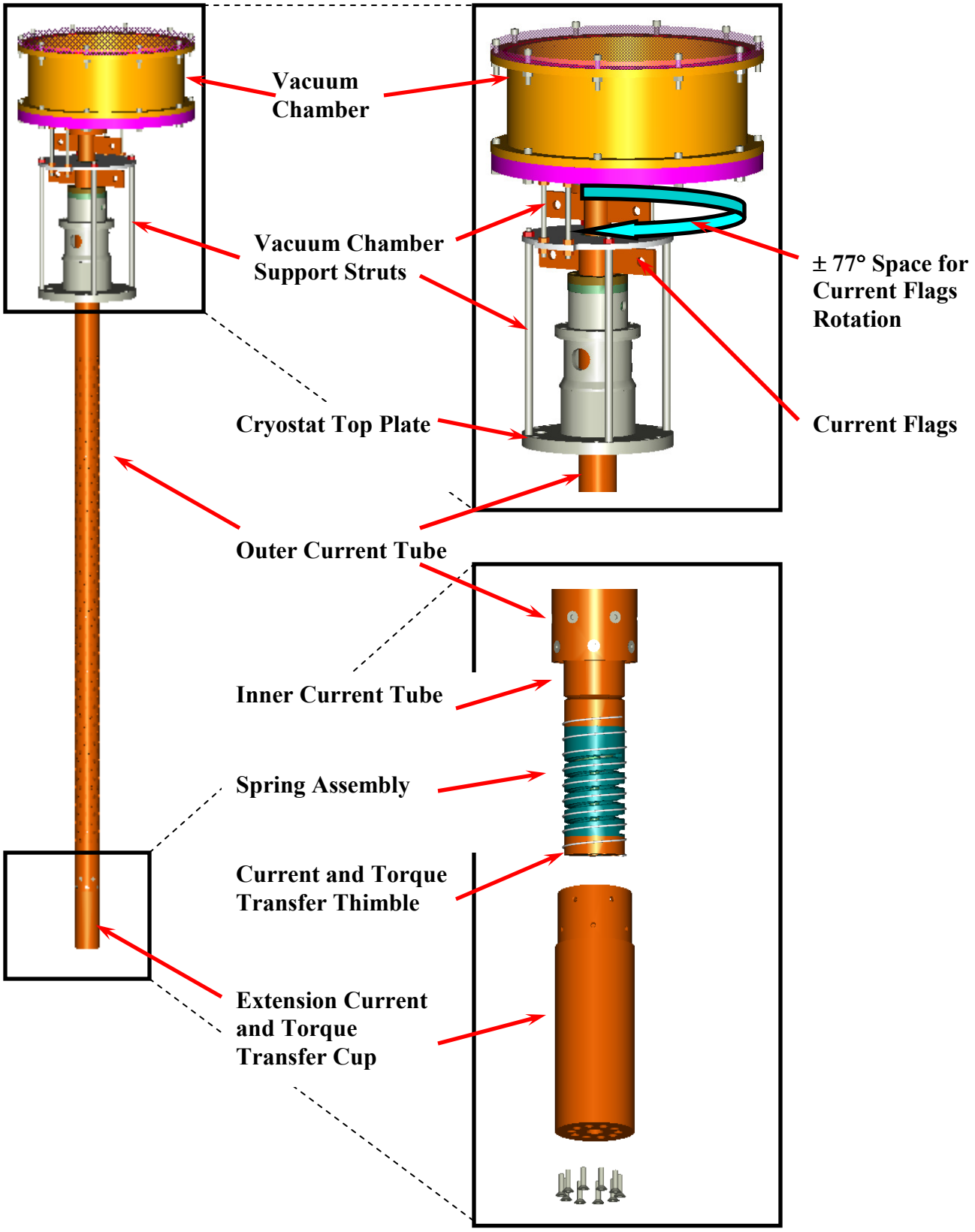

Figure 13. Full assembly of probe

4.0 Resistance Calculations:

The probe assembly has many interconnections and in order to ensure that the current is being fully transmitted to and from the sample without much loss the gap or junction resistances at the interconnections have to be low enough. Studies [14] were conducted in the past on similar probes to correlate current and contact resistance and it has been shown that a resistance of 1 μΩ or lower is needed for a current of 2000 A to be transported at liquid helium temperatures through the sample. The contact and splice resistances for the different junctions have been calculated using the methodology described in [14].

4.1 Contact Resistance:

Contact resistance between two bodies is due to two factors, constriction resistance and contaminant resistance. The constriction resistance is due to the existence of surface asperities (surface roughness) and thus the true load bearing area A_b would be much less than the apparent contact area A_a that would exist in the absence of asperities. The force by which these bodies are held together plays an important role by flattening the asperities (humps), increasing the contact area and thus reducing the constriction resistance. The constriction resistances at the outer current tube and the extension cup interface (figure 14, (a)) and also at the base, i.e. extension cup and copper thimble (figure 14, (b)) interface were analytically determined assuming no contamination at the interface.

The interfaces are held together by screws and we assume a tightening torque of 1 N.m. per screw. For a standard steel nut [15] assuming a friction coefficient of 0.15 the force transmitted to the interface by the screw can be given by:

$$F = \frac{T}{0.2D} \tag{8}$$

where,

T – Tightening torque

D – Nominal thread diameter of the screw/bolt

Since the material of the contacting bodies is the same there is no relative thermal contraction between them, the small contribution from the screw can be neglected.

According to [14] the asperities can be assumed to be humps of spherical segments with an average diameter, d of 4 microns and a radius of curvature, r of 0.4 micron.

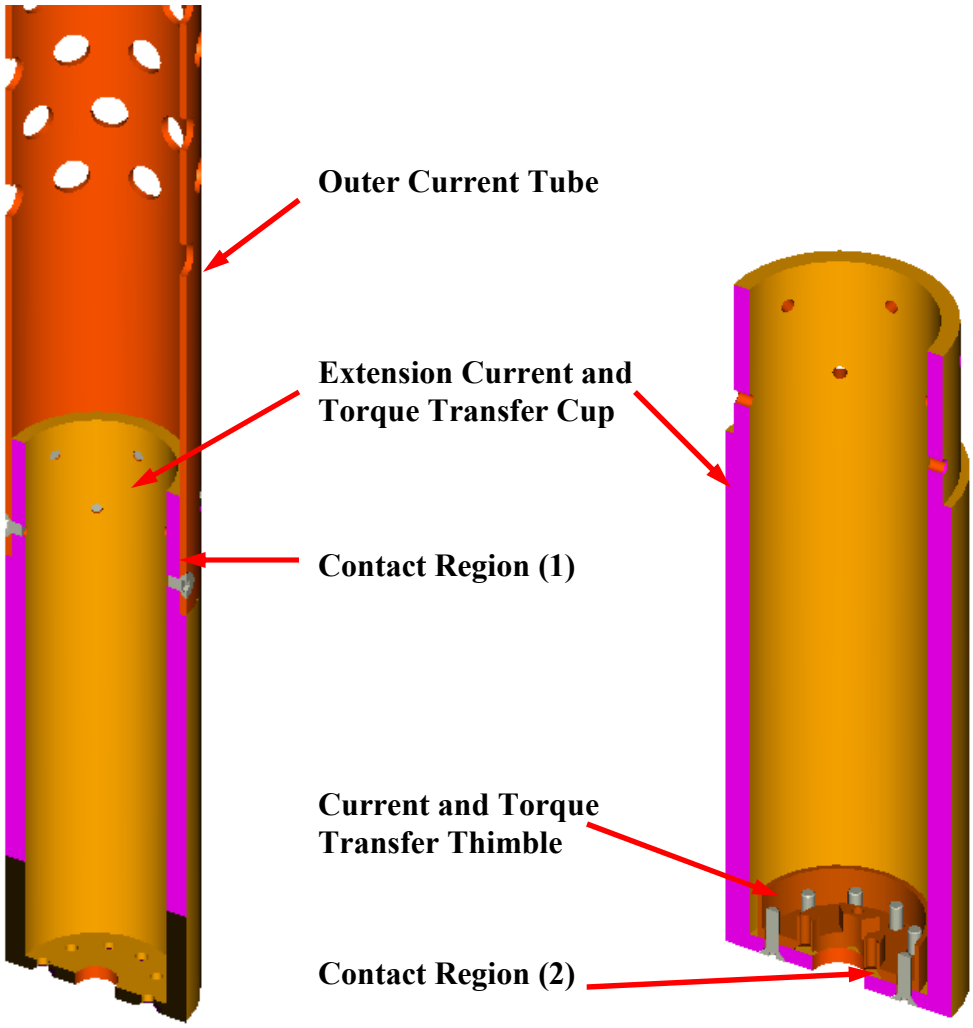

(a) (b)

Figure 14. Interfaces contributing to resistance of current flow

The humps cannot lie closer than one per area of d^2 and thus the average pressure on the apparent contact area is given by:

$$Pa = \frac{F}{Aa} \tag{9}$$

The average load per hump is given by:

$$Pi = Pa * d2 \tag{10}$$

Considering a purely elastic deformation for a ball contacting a semi-infinite plane body of the same material the Poisson's ratio is 0.3, which is valid for iron, nickel and copper. The diameter of a single spot is given by:

$$a = 1.11\sqrt[3]{\frac{Pi}{E}}.r \tag{11}$$

where, E – Elastic modulus of the material, copper in our case.

The average pressure in the load bearing area is given by:

$$p = \frac{\int_0^a \frac{1.5.Pi}{\pi.a^3}.\sqrt{a^2 - x^2}.dx}{a} \tag{12}$$

The true load bearing area can be determined as following:

$$A_b = \frac{Pa}{P} A_a \tag{13}$$

Assuming that the humps are far enough from each other as to contribute individually to the constriction resistance, the individual conductance can be summed. The total constriction resistance can thus be calculated as below:

$$R = \frac{\rho}{4.A_b} \tag{14}$$

where, ρ is the residual resistivity of the material. The constriction resistances determined using equation (14) for the different interfaces was found to be less than 1 μΩ. The detailed calculations for the contact regions (1) and (2) shown in figure 14 are presented in appendix 3.

4.2 Splice Resistance:

The superconductor sample under investigation experiences a resistance to the current flow at the input and output, i.e. where the current is supplied and where it is drawn from. This resistance contribution is from the joint resistance of the solder between the sample and the copper leads and can be investigated and determined by considering a section or splice model as described in [16]. The loss will be minimized by having more turns soldered and it is recommended to maintain this resistance value in the nano-ohm levels.

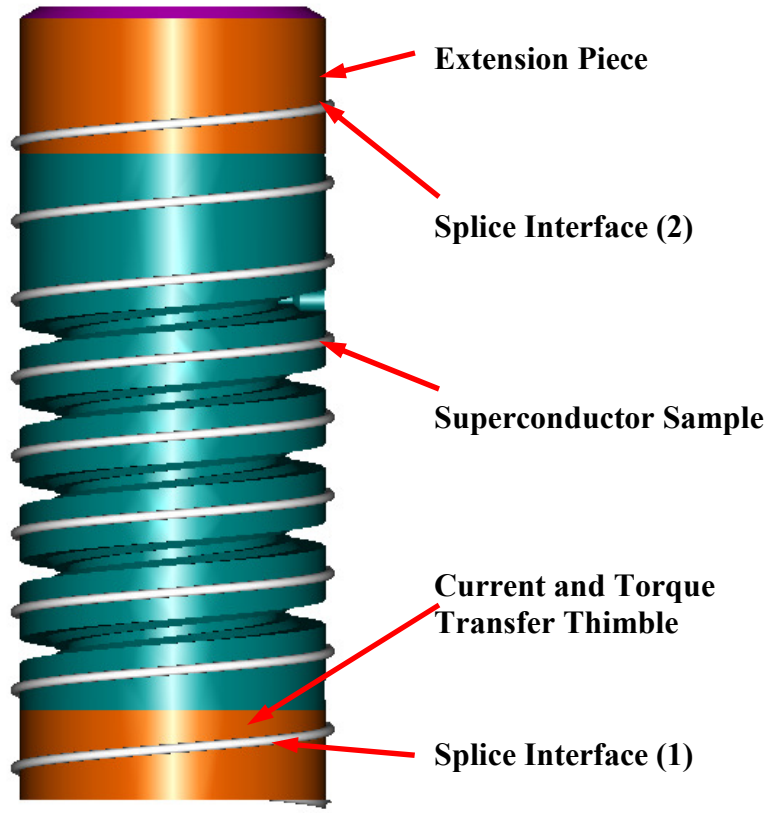

Figure 15. Image showing the splice interface regions.

In our case splice resistances exist at the solder joint between the current and torque transfer thimble and the sample at the bottom of the spring and also between the extension piece and sample at the top of the spring as shown in figure 15. Two turns of the sample will be soldered at each end and for simplicity of calculations the length of the joint is considered to be homogenous and is equal to twice the diameter of the sample. As the helix angle is very small (figure 15 shows a larger pitch) the sample can be assumed to be perpendicular to the sample axis.

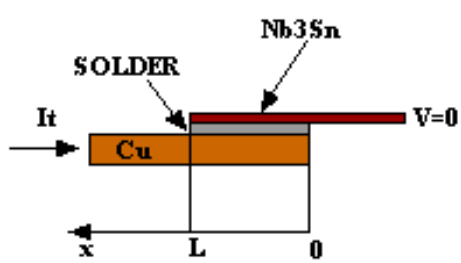

Figure 16. Model for the estimation of joint resistance [14].

Considering the current flow direction as shown in figure 16 the junction resistance can be calculated as follows:

The resistance per unit length of the copper is given by:

$$R = \frac{\rho_{Cu}.L}{\pi.d_{Cu}.t_{Cu}} \tag{15}$$

The contact resistance across the solder, per unit length in the x-direction is given by:

$$r = \frac{\rho_{Sr}.t_{Sr}}{\pi.d_{Sr}.L} \tag{16}$$

where,

ρ_{Cu} and ρ_{Sr} are the resistivities,

t_{Cu} and t_{Sr} are the thicknesses,

d_{Cu} and d_{Sr} are the diameters of copper and solder, respectively and L is the length and is considered as unity in the calculations.

Thus the voltage of copper relative to the superconductor is given by:

$$V(x) = r\frac{dI(x)}{dx} \tag{17}$$

and

$$\frac{dV(x)}{dx} = I(x).R \tag{18}$$

The voltage is taken to be uniform at V=0. Solving equations (17) and (18) for zero and maximum current, we get:

$$V(x) = I_t(R.r)^{1/2}\frac{e^{\alpha x} + e^{-\alpha x}}{e^{\alpha L} - e^{-\alpha L}} \tag{19}$$

where $\alpha = (R/r)^{1/2}$ and I_t is the maximum current, 2000 A in our case.

The voltage at L can be obtained from equation (19) by substituting L = 2 mm, length for 2 turns and consequently the junction resistance is obtained as follows:

$$R_j = \frac{V_L}{I_t} \tag{20}$$

The detailed calculations are shown in appendix 3 and the junction resistances at the two interfaces were found to be in the order of nano-ohms.

5.0 Current Lead Optimization

The outer and inner tubes or leads carry the current from an external DC power source to and from the test sample and at any time are expected to carry a current of 2000 A. The portion of the leads outside the cryostat that is exposed to the outer environment carries the heat from the atmosphere into the cryostat resulting in the evaporation of the liquid helium. In order to minimize the rate of evaporation of helium whilst keeping the leads sufficiently cool the thermal design of the leads was considered.

5.1 Thermal Model:

Heat transfer occurs due to conduction of heat from the warm end (top surface) of the leads to the cold end (portion immersed in helium), due to evaporation of liquid helium and due to the convection between the helium vapor and the current lead surface. There is also heat generation from within the system due to the joule's heating caused by the flow of current. This heat generation term depends on the temperature dependent resistivity of the lead material. Neglecting the effects of radiation, the time dependent behavior of the system can be described by the following PDEs [14].

$$\frac{\partial}{\partial x}\left[k(T)\frac{\partial T}{\partial x}\right]+\frac{\rho(T)I^2(t)}{A^2}-\frac{hp}{A}(T-\vartheta)=C_p(T)\delta(T)\frac{\partial T}{\partial t} \tag{21}$$

$$\frac{hp}{A_v}(T-\vartheta)-\frac{\dot{m}C_p^v(\vartheta)}{A_v}\frac{\partial\vartheta}{\partial x}=C_p^v(\vartheta)\delta^v(\vartheta)\frac{\partial\vartheta}{\partial t} \tag{22}$$

Where,

T = Cu temperature, [K]

ϑ = He vapor temperature, [K]

p = cooled perimeter, [m]

A= Cu cross section, [m^2]

Aν = He vapor cross section, [m^2]

I = current, [A]

K(T) = Cu thermal conductivity, [W/ cm K]

ρ(T) = Cu electrical resistivity, [Ω. Cm]

C_p^v = He vapor specific heat, [J/g K]

C_p = Cu specific heat, [J/g K]

$\delta(T)$ = Cu density, [g/cm^3]

$\delta^v(T)$ = He vapor density, [g/cm^3]

h = heat transfer coefficient, [W/cm^2 K]

m = He vapor mass flow rate, [g/s]

For steady state conditions, i.e. constant current, the equations become:

$$\frac{\partial}{\partial x}\left[k(T)\frac{\partial T}{\partial x}\right]+\frac{\rho(T)I^2(t)}{A^2}-\frac{hp}{A}(T-\vartheta)=0 \tag{23}$$

$$\frac{hp}{A_v}(T-\vartheta)-\frac{\dot{m}C_p^v(\vartheta)}{A_v}\frac{\partial\vartheta}{\partial x}=0 \tag{24}$$

The heat flux into the liquid He bath from the leads is given by:

$$Q=\sum A_{cu}k_{4.2}\frac{\partial T}{\partial x}_{x=0} \qquad \text{in W} \tag{25}$$

The rate of evaporation of helium is given by:

$$\dot{m}=\frac{dm}{dt}=\frac{Q}{\Delta h} \qquad \text{in g/s} \tag{26}$$

where Δh is the latent heat of evaporation of helium.

5.2 Lock's Optimization:

The geometry of the current lead plays an important role in the thermal efficiency of the system. A smaller lead cross section reduces the conduction of heat into the system but also increases the resistance and thereby the joule's heat generation and the inverse effects are true for larger cross sections. For a given value of current through the lead, there exists an optimal length to cross section ratio which will minimize the heat leak into the system and also reduce the boil-off of liquid helium.

J. M. Lock [17] proposed an optimization procedure for copper leads based on the general solution of the problem of a current lead in good thermal exchange with an evaporating cryogenic fluid. For steady state flow, all the heat entering or created in an element 'dx' of the lead (shown in figure 17) must be transferred to the gas and thus the heat flow equation becomes:

$$dQ+\frac{\rho I^2}{A(x)}dx=nC_p dT \tag{27}$$

where,

n – moles per second of the evaporating gas

A(x) – cross section area of the lead

ρ – resistivity of the copper lead

C_p – molar specific heat of the gas at constant pressure

Q – heat flow by conduction down the conductor

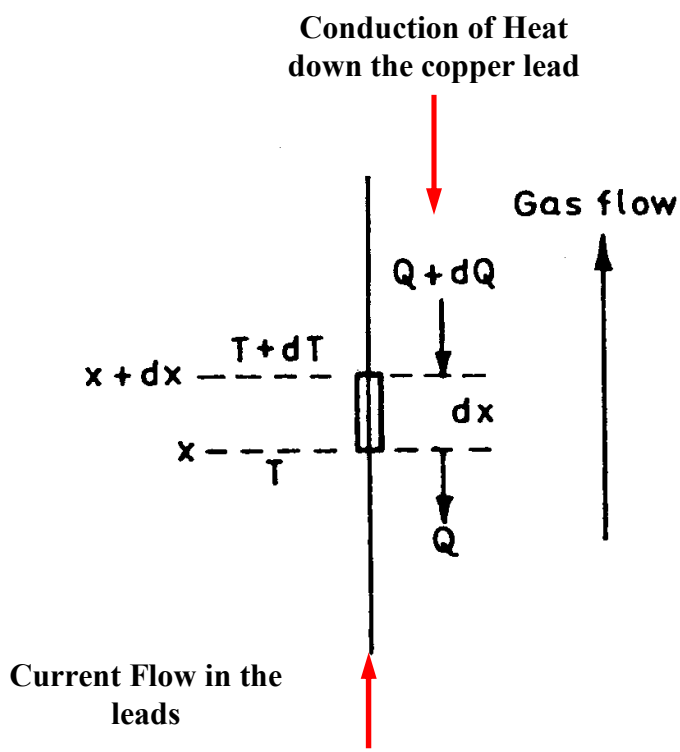

Figure 17. Schematic model of an elemental length of lead showing the direction of heat flow [17].

The heat flow due to conduction is given by:

$$Q = \kappa A(x)\frac{dT}{dx} \tag{28}$$

Using eqn. (28) and assuming that the heat flow down the conductor is the only source of evaporation of the cryogenic fluid, equation (27) can be solved.

Lock's results give an optimized lead geometry given the residual resistivity of the material (shown in figure 18). Since the residual resistivity is a parameter that can vary largely from sample to sample, a good knowledge of the lead material properties is necessary for the design. We chose a commonly available copper lead with a RRR = 100

(i.e. the residual resistivity ratio is 100) for which the residual resistivity is 1.69 e-9 Ω cm. The warm end of the current lead is considered to be at 300 K.

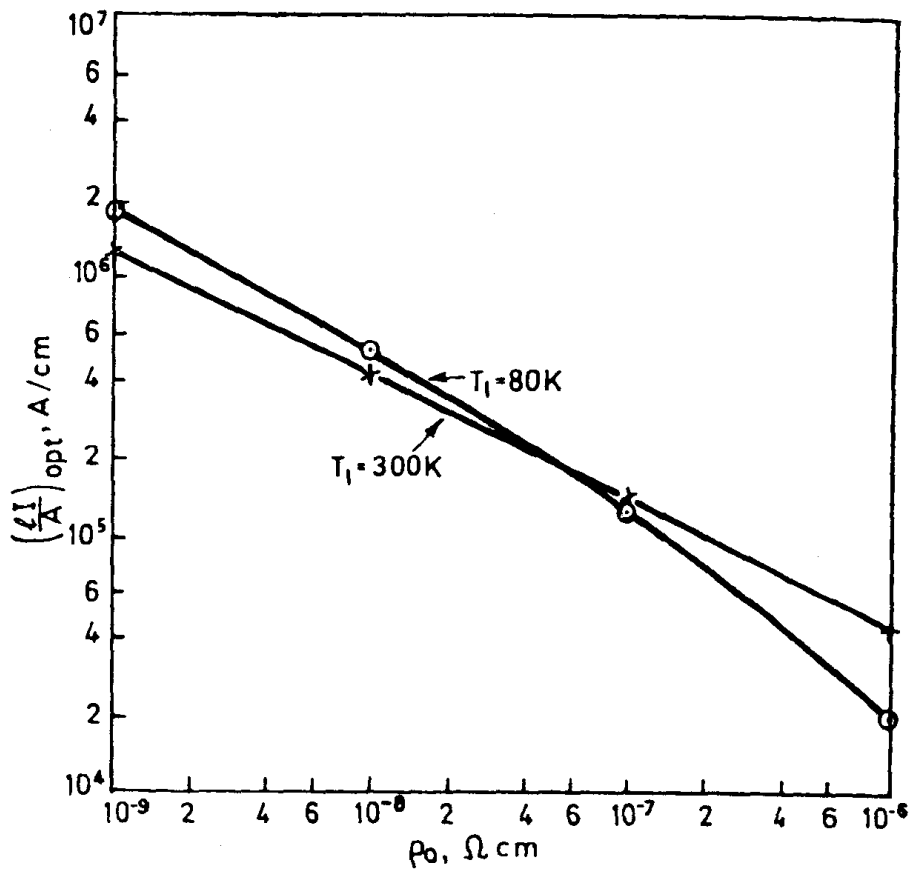

Figure 18. Result from Lock's analysis showing relationship between lead geometry and residual resistivity.

From the above plot, given the resistivity and warm end temperature we obtain the optimal geometry parameter: $\left(\frac{lI}{A}\right)_{opt} = 3.3e5\frac{A}{cm}$

The length of the lead cooled by helium vapor is l = 100 cm, the current is 2000 A and thus the optimal cross section area is Aopt = 0.606 cm^2. Table 3 gives the dimensions of the current lead and their cross sectional areas and as can be seen the actual cross sectional areas are much larger than the optimal section required. To have efficient cooling holes were drilled on the tubes to reduce the cross sectional areas. A simple geometrical consideration of a circular annulus was considered to determine the number

and size of the holes that could be cut from the tube. From prior experience [14] it was found that the distance between adjacent holes should be at least twice their diameter and the ratio of the volumes of the leads with and without the holes should be close to unity. The detailed calculations are presented in Appendix 4.

Geometrical Parameter	Outer Current Lead	Inner Current Lead
Outer Diameter (cm)	4.445	3.175
Inner Diameter (cm)	4.115	2.54
Cross Sectional Area (cm^2)	2.219	2.849

Table 3. Geometry of current leads

5.3 LEADX Simulation:

LEADX is a program [18] that helps simulate the behavior of current leads. It is an iterative solver, which solves equations (23) and (24) for either copper or brass material. The program begins with an initial assumption for the mass flow rate of the cooling gas and given geometry to iteratively arrive at the accurate solution. The following are the parameters that were used in the simulation.

M-flow, mass flow rate of cooling gas	0.0008	Kg/sec
Current, Total current in the leads	4000	amp
Length, Length of gas cooled lead	1	m
Perimeter, cooling surface of the lead/ unit length	0.449	m
C-area, conductor cross sectional area	0.0005	m^2
RRR, residual resistivity ratio of lead	100	
Iteration, number of iterations	300	
Effect dia., effective diameter of gas path	0.042	m
Warm end temp, temp. at warm end of lead	300	K
Cold end temp, temp. at cold end of lead	4.2	K

Figure 19 shows the plot of the temperature profile along the lead obtained from this simulation. The profile shows a smooth transition of a polynomial curve from the cold end to the warm end without any jumps or discontinuities which confirms that the design will not lead to any instabilities or thermal run off in the system.

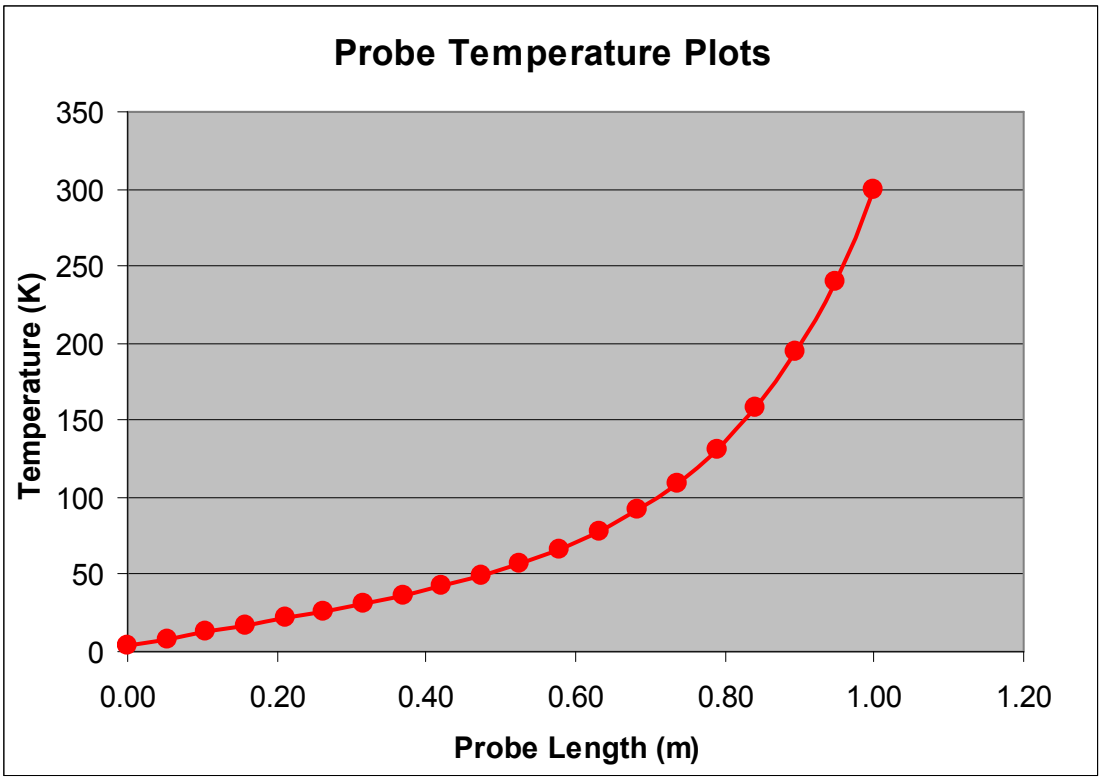

Figure 19. Temperature profile in the lead for a warm end temperature of 300 K using LEADX simulation.

6.0 Structural Analysis

The major mechanical load in the system is the torsion applied to the test sample. This torque is transmitted from the gear box to the sample via the inner current lead and eventually to the outer current lead. The inner lead is not constrained and is free of stresses, while the outer current lead and all the torque transmitting dowel pins and screws will experience shear stresses due to this torsion.

6.1 Torsion of Outer Tube:

The outer tube is subjected to a torque at the bottom while the top end is fixed. This loading scenario is that of a hollow cylinder fixed at one end and subjected to a torque at the other end, only the problem is complicated due to the holes that will be drilled in the tube for thermal design. Nonetheless the calculations were performed by reducing the cross section by 50% (a very conservative assumption) and it was found that the stresses are within safe operating limits. The detailed calculations are presented in

appendix 5. A finite element analysis was also performed to verify the analytical solution. Figure 20 shows the plot of the von mises stresses in the tube. The stresses in the body of the tube are around 14 MPa as predicted from the analytical calculations. There are stress concentrations near the holes as expected although the values lie well below the shear yield limit for copper of 88 MPa.

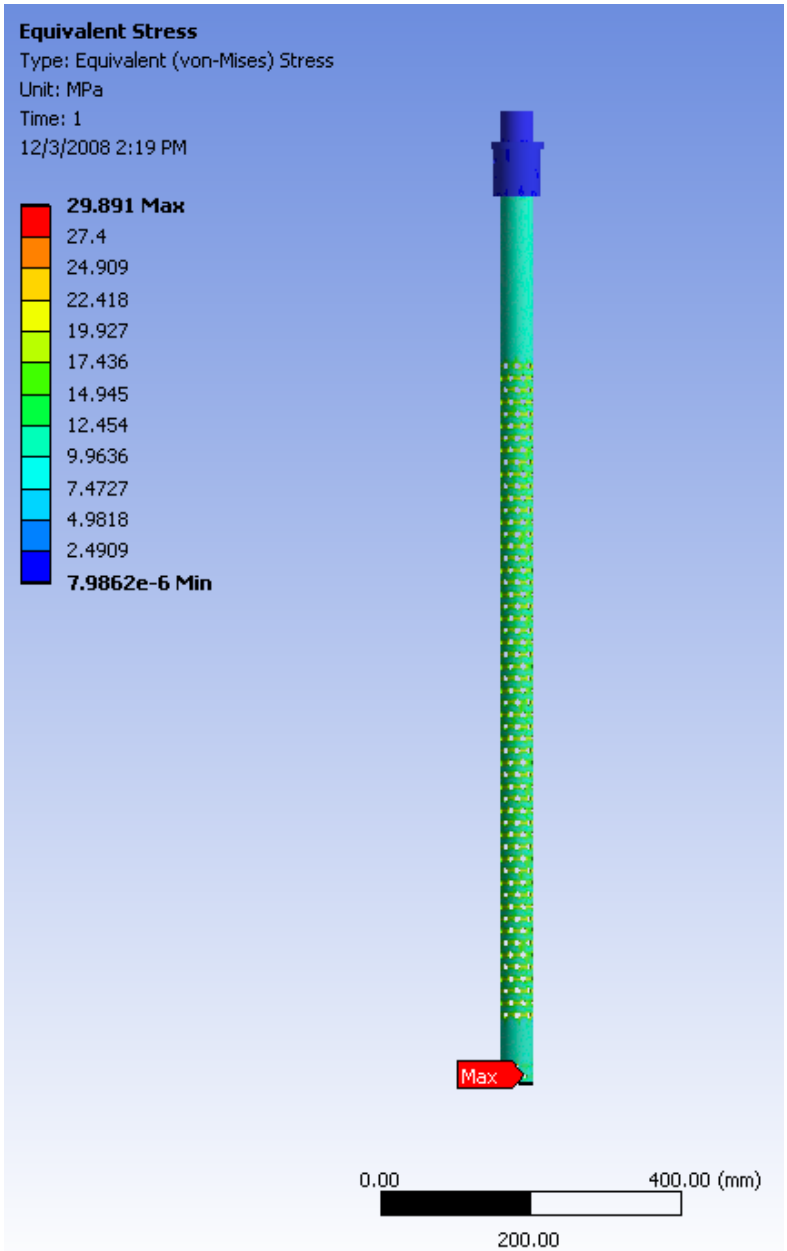

Figure 20. Plot of von-mises stresses in the outer current tube

6.2 Shear Stresses in Pins/Bolts:

The dowel pins and bolts that transfer the torque are assumed to be under pure torsion and thus under direct shear stress. The shear stresses are found by the simply dividing the force exerted by the cross sectional area of the pin or bolt. In the case of bolts the diameter corresponding to the stress area is used. The shear yield of the material is assumed to be 40% of the tensile yield strength. The calculations show that all the pins and fasteners are being operated within the safe loading limits. The detailed calculations are shown in appendix 5.

7.0 Summary

A probe to perform strain sensitivity studies on LTS wires and HTS wires and tapes was designed. The probe uses a modified version of the Walter's spring device for the mounting of the sample and application of strain. The helical spring was designed based on the methodology described by Walters' et al. and Taylor et al. and is able to handle both wires and tapes. The measurements will be performed on two different spring materials: Ti-6Al-4V and Beryllium copper (CuBe). The design allows the Ti-6Al-4V spring to reach strain levels of ± 0.8 % and the CuBe to reach ± 0.7 %. Finite element analysis of the spring was performed and the results are promising, the strains are within 5% of the analytical solution and a sinusoidal oscillation of the strains along the helix was observed similar to that described by Taylor et al. The spring has 4 turns and total height of 64.25 mm.

The probe was designed to fit an existing setup used to perform critical current density studies. The sample to be tested is mounted on the spring and the strain is applied using a hand operated worm gear setup. The angular displacement of the spring is measured by means of a protractor and pointer as described in section 3. The gear box is contained within a vacuum chamber to protect it from moisture and dirt. The worm gear can handle a torque of ~ 60 N. m. The design allows for the change in length of the spring that occurs as the spring is strained by means of dowel pins.

The current leads which are also the torque transferring members are designed and optimized using the methodology described by J. M. Lock for copper leads in a cryostat. The leads are capable of handling a current of 2000 A. The interconnections and

joints in the assembly were designed to have minimum contact resistance to allow efficient flow of current.

Finally the mechanical soundness of the system was also verified by performing calculations to ascertain that the stresses in the structural members and pins and fasteners were within the safe operating limits.

Acknowledgements

The author wishes to thank E. Barzi and her lab for the technical guidance and extensive support on this project. The author wishes to acknowledge the design support of K. Ewald. The author also wishes to thank S. Tariq for the help with ANSYS simulations. Thanks also to D. Markewicz, NHMFL and N. Cheggour, NIST, and M. Gedeon, Brush Wellman Inc., for the helpful information. The author wishes to thank the support of the TD-Magnet Systems Department, TD-D&D group and the TD-SRF group and also the help of the TD-QM Department.

References:

[1] D. M. J. Taylor and D. P. Hampshire, "Properties of helical springs used to measure the axial strain dependence of the critical current density in superconducting wires", Supercond. Sci. Technol. 18 (2005) 356-368.

[2] B. ten Haken, A. Goedke and H. H. J. ten Kate, "The strain dependence of the critical properties of Nb_3Sn conductors", J. App. Physics, 1999, vol. 85(6).

[3] H. J. N. van Eck et al., "Critical current versus strain research at the university of Twente", Supercond. Sci. Technol. 16 (2003) 1026-1030.

[4] H. Kitaguchi et al., "Critical current of magnesium diboride/stainless steel composite tapes under tensile or compressive strains", Supercond. Sci. Technol. 16 (2003) 976-979.

[5] A. Godeke et al., "A device to investigate the axial strain dependence of the critical current density in superconductors", Rev. Sci. Instrum., Vol. 75, No. 12, Dec 2004.

[6] C. R. Walters et al., "Long sample high sensitivity critical current measurements under strain", Cryogenics, 1986 vol. 26, 406-412.

[7] N. Cheggour and D. P. Hampshire, 'A probe for investigating the effects of temperature, strain, and magnetic field on transport critical currents in superconducting wires and tapes", Rev. Sci. Instrum., Vol. 71, No. 12, Dec 2000.

[8] B. Seeber et al., "Critical current versus strain measurement up to 21 T and 1000 A of long length superconducting wires and tapes", Rev. Sci. Instrum., 76, 093901 (2005).

[9] W. Turner, "Electroplating of titanium and titanium base alloy", U.S. patent 4416739, Nov. 1983.

[10] C. E. Fuller and W. A. Johnston, "Applied mechanics", Vol. II Strength of Materials, copyright 1919, p. 398.

[11] D. Uglietti et al., "A device for critical current versus strain measurements up to 1000 A and 17 T on 80 cm long HTS and LTS technical superconductor", Supercond. Sci. Technol. 16 (2003) 1000-1004.

[12] F. R. Schwartzberg, "Cryogenic materials data handbook", Air force materials laboratory, Technical documentary report, AFML-TDR-64-280, Vol. I, July 1970.

[13] Brush Wellman Inc., private communication.

[14] L. Del Frate, "Design of a low resistance sample holder for instability studies of superconducting wires", University of Pisa, Thesis 2004.

[15] R. C. Juvinall, K. M. Marshek, "Fundamentals of machine component design", 4th edition, p. 410.

[16] M. N. Wilson, "Superconducting magnets", 1983, ISBN 0198548109, p. 234.

[17] J. M. Lock, "Optimization of current leads in a cryostat", Cryogenics, Dec 1969.

[18] M. Wake, "LEADX note", Software manual, KEK, Japan.

Appendix 1

Optimization Procedure for Helical Spring Cross Section

Proposed by Walters' et al. [6], adapted by Taylor et al. [1]

Step 1. Maximize the outer diameter of the spring:

Outer diameter, mm	D := 31.75
Outer radius, mm	r1 := 15.875

Step 2. Maximize the width of the section inside:

Pitch of the spring between turns is about 1/4 of outer diameter, mm	p := 8
Width inside is 0.8 times pitch, mm	w2 := 7

Step 3. Minimize the width of the section outside:

Width is chosen to accommodate wires of dia 1mm and tapes of max. width 4.7 mm	w1 := 5.5

Step 4. Assume r2 and step position to minimize rn and strain ratio:

Inner radius of the spring, mm	r2 := 11
Step position of the spring, mm	sp := 12.5

To find the optimal neutral radius (rn) :

Neutral radius can be found by evaluating the integral shown below:

$$\int w(r)E(r)\varepsilon_{\theta\theta}(r)dr = 0$$

The integral is evaluated over the 3 regions of the cross section

Integral limits for the different sections

$$\int_{11}^{12.5} 7\cdot\left(1-\frac{rn}{r}\right)dr \rightarrow rn\cdot(7\cdot\ln(11)-17.6801005101577880)78+10.5$$

i.e. 10.5 - 0.89 rn

upper limit for the second integral, mm

$$b1 := sp + \frac{(w2-w1)}{2}$$

$$b1 = 13.25$$

width is eqn of tapered line with -ve slope and intercept sum of co-ords, 12.5+7

$$\int_{12.5}^{13.25} (19.5-r)\cdot\left(1-\frac{rn}{r}\right)dr \rightarrow -0.3862437084175276227\,rn + 4.9687$$

i.e. 4.97 - 0.39 rn

$$\int_{13.25}^{15.875} 5.5\cdot\left(1-\frac{rn}{r}\right)dr \rightarrow -0.9941139579058827121\,rn + 14.437$$

i.e. 14.44 - 0.99 rn

Equating the total integral to zero, we get 10.5+4.97+14.44 = (0.89+0.39+0.99)rn

Therefore neutral radius in mm

$$rn := \frac{(10.5+4.97+14.44)}{0.89+0.39+0.99} \qquad rn = 13.176$$

To calculate strain ratio

Angular displacement, radians $\theta := 68 \cdot \frac{3.14}{180}$

$\theta = 1.186$

Number of turns in the spring $N := 4$

Helix angle of the spring, radians $\alpha := 7.18 \cdot \frac{3.14}{180}$

$\alpha = 0.125$

Strain eqn. factor $K := \frac{\theta \cdot \cos(\alpha)}{2 \cdot 3.14 \cdot N}$

$K = 0.047$

Strain at the inner surface $\varepsilon i := K \cdot \left(1 - \frac{rn}{r2}\right)$

$\varepsilon i = -9.269 \times 10^{-3}$

Strain at the outer surface $\varepsilon o := K \cdot \left(1 - \frac{rn}{r1}\right)$

$\varepsilon o = 7.965 \times 10^{-3}$

Strain ratio $\varepsilon r := \frac{-\varepsilon i}{\varepsilon o}$ $\varepsilon r = 1.164$

Torque required

The torque required to produce a certain strain value can be calculated as follows:

1. Specify a strain constraint, in our case we want to achieve 0.8% strain at the outer surface

The torque is given by:

$$T = \frac{\sigma_o . A . e . r_o}{C_o}$$

Young's modulus of Ti6Al4V at 4.2 K, MPa $\quad Et := 13000($

Young's modulus of CuBe at 4.2 K, MPa $\quad Ec := 13200($

Stress at the outer surface, MPa $\quad \sigma oc := 0.008 \cdot Ec \quad \sigma ot := 0.008 \cdot Et$

$\sigma oc = 1.056 \times 10^3 \quad \sigma ot = 1.04 \times 10^3$

To calculate centroid and area of cross section

	section	width	height	area	ybar	xbar	a*ybar	a*xbar
	1	7	1.5	10.5	11.75	4	123.375	42
	2	5.5	0.75	4.125	12.875	4	53.1094	16.5
	3	5.5	2.625	14.4375	14.5625	4	210.246	57.75
	4	0.75	0.75	0.28125	12.75	1	3.58594	0.28125
	5	0.75	0.75	0.28125	12.75	7	3.58594	1.96875
	summation			**29.625**			**393.902**	**118.5**

Centroid of the section, mm $\quad ybar := \frac{393.902}{29.625} \quad ybar = 13.296$

$xbar := \frac{118.5}{29.625} \quad xbar = 4$

Area of cross section, mm^2 $\quad A := 29.62$

Distance from neutral axis to outer surface, mm $Co := -(r2 - rn)$ $Co = 2.176$

Eccentricity, mm $e := ybar - rn$ $e = 0.12$

Torque required, N.m. $Tt := \frac{(\sigma ot \cdot A \cdot e \cdot r1)}{Co \cdot 1000}$

For Ti6Al4V spring, N.m. $Tt = 26.983$

$Tc := \frac{(\sigma oc \cdot A \cdot e \cdot r1)}{Co \cdot 1000}$

For CuBe spring, N.m. $Tc = 27.399$

Appendix 2

Analytical Solution for Torsion of Helical Spring with T-Shaped Cross Section

Formula from applied mechanics, Fuller and Johnston, MIT, 1919

Number of turns in the spring $n := 4$

Mean diameter, mm $D := 13.2963 \cdot 2$

Helix angle, radians (corresponds to 7.18 degrees) $\theta := \frac{(7.18 \cdot 3.14)}{180}$

total length of helix, mm $l := \frac{(n \cdot 3.14 \cdot D)}{\cos(\theta)}$ $l = 336.64$

Moment of inertia about y axis, mm^4 $I := 59.62$

Polar moment of inertia, mm^4 $Ip := 100.2$

Young's modulus of Ti alloy at 4.2K, N/mm^2 $E := 13200($

Poisson's ratio at 4.2K $\nu := 0.31$

Shear modulus at 4.2K, N/mm^2 $G := \frac{E}{2 \cdot (1 + \nu)}$

$G = 5.038 \times 10^4$

Parameter $K1 := \frac{(\sin(\theta) \cdot \sin(\theta))}{(G \cdot Ip)}$ $K1 = 3.091 \times 10^{-9}$

$K2 := \frac{(\cos(\theta) \cdot \cos(\theta))}{E \cdot I}$ $K2 = 1.251 \times 10^{-7}$

Summation of parameters $K := K1 + K2$ $K = 1.282 \times 10^{-7}$

If applied torque is, N mm $M := 3000($

Angle of twist, rad $\phi := M \cdot l \cdot K$ $\phi = 1.294$

Angle of twist, deg $\phi d := \frac{(\phi \cdot 180)}{3.14}$ $\phi d = 74.205$

To calculate angular rotation about spring section axis

Parameter $K3 := \frac{(\cos(\theta) \cdot \sin(\theta))}{(G \cdot Ip)}$

$K3 = 2.455 \times 10^{-8}$

$K4 := \frac{(\sin(\theta) \cdot \cos(\theta))}{E \cdot I}$

$K4 = 1.575 \times 10^{-8}$

$KII := K3 - K4$

$KII = 8.803 \times 10^{-9}$

$\omega := M \cdot l \cdot KII$

Rotation about spring axis $\omega = 0.089$

Total change in length, mm $\delta := \frac{(D \cdot \omega)}{2}$ $\delta = 1.182$

Appendix 3

Resistance Calculations - Contact Resistance

Contact Region (1) – Outer Current Tube and Extension Cup Interface

Assume tightening torque on the screw for a total of 12 screws, N.m $T := 12$

Screw size (nominal diameter), metric, m $D := 3 \cdot 10^{-3}$

Co-efficient of friction $\mu := 0.15$

Force, N $F := \frac{T}{0.2 \cdot D}$ $F = 2 \times 10^{4}$

Ignore stresses due to thermal contraction, same material

Inner diameter of the outer tube, m $di := 1.625 \cdot 25.4 \times 10^{-3}$ $di = 0.041$

Height of end cap in contact, m $l := 30 \cdot 10^{-3}$ $l = 0.03$

Apparent contact area, m^2 $Aa := 3.14 \cdot di \cdot l$ $Aa = 3.888 \times 10^{-3}$

Average pressure, Pa $Pa := \frac{F}{Aa + 2.14 \cdot 10^{-4}}$ $Pa = 4.876 \times 10^{6}$

Average load per hump, N $Pi := Pa \cdot \left(4 \cdot 10^{-6}\right)^{2}$ $Pi = 7.801 \times 10^{-5}$

Elastic modulus of copper, Pa $E := 110 \cdot 10^{9}$

Radius of the hump, m $r := 4 \cdot 10^{-5}$

contact area of single spot, m $a := 1.11 \cdot \left[\sqrt[3]{\frac{(Pi \cdot r)}{E}}\right]$ $a = 3.385 \times 10^{-7}$

Value of integral	$Int := \frac{\left(a^2 \cdot 1.57\right)}{2}$	$Int = 8.996 \times 10^{-14}$
Numerator in the avg. pr expression	$Nr := \frac{(1.5 \cdot Pi \cdot 1.57)}{3.14 a \cdot 2}$	$Nr = 86.413$
Average pressure in the load bearing area, Pa	$p := \frac{Nr}{a}$	$p = 2.553 \times 10^{8}$
Ratio of avg. pressures	$Rt := \frac{p}{Pa}$	$Rt = 52.356$
True load bearing area, m^2	$Ab := \frac{Aa}{Rt}$	$Ab = 7.426 \times 10^{-5}$
Residual resistivity, Ω.m	$\rho := 1.68 \cdot 10^{-10}$	
Total constriction resistance, Ω	$R := \frac{\rho}{4 \cdot Ab}$	$R = 5.656 \times 10^{-7}$

Contact Region (2) –Extension Cup and Copper Thimble Interface

Assume tightening torque on the screw for 10 screws, N.m	$T := 10$
Screw size (nominal diameter), metric, m	$D := 2.5 \cdot 10^{-3}$
Co-efficient of friction	$\mu := 0.15$
Force, N	$F := \frac{T}{0.2 \cdot D}$

Ignore stresses due to thermal contraction, same material

Outer diameter of the ring, m	$do := 1.25 \cdot 25.4 \times 10^{-3}$	$do = 0.032$
Inner diameter of the ring, m	$di := 11 \cdot 10^{-3}$	$di = 0.011$
Apparent contact area, m^2	$Aa := 3.14 \cdot \left[\left(\frac{do}{2}\right)^2 - \left(\frac{di}{2}\right)^2\right]$	
	$Aa = 6.963 \times 10^{-4}$	
Area of flat head screws, m^2	$af := \frac{3.14 \cdot 5.5^2 \cdot 10 \cdot 10^{-6}}{4}$	$af = 2.375 \times 10^{-4}$
Average pressure, Pa	$Pa := \frac{F}{Aa - af}$	$Pa = 4.358 \times 10^{7}$
Average load per hump, N	$Pi := Pa \cdot \left(4 \cdot 10^{-6}\right)^2$	$Pi = 6.973 \times 10^{-4}$
Elastic modulus of copper, Pa	$E := 110 \cdot 10^{9}$	
Radius of the hump, m	$r := 4 \cdot 10^{-5}$	
Contact area of single spot, m	$a := 1.11 \cdot \left[\sqrt[3]{\frac{(Pi \cdot r)}{E}}\right]$	$a = 7.026 \times 10^{-7}$
Value of integral	$Int := \frac{\left(a^2 \cdot 1.57\right)}{2}$	$Int = 3.875 \times 10^{-13}$
Numerator in the avg. pr expression	$Nr := \frac{(1.5 \cdot Pi \cdot 1.57)}{3.14 \cdot a \cdot 2}$	$Nr = 372.208$
Average pressure in the load bearing area, Pa	$p := \frac{Nr}{a}$	$p = 5.298 \times 10^{8}$
Ratio of avg. pressures	$Rt := \frac{p}{Pa}$	$Rt = 12.155$

True load bearing area, m^2	$Ab := \frac{Aa}{Rt}$	$Ab = 5.729 \times 10^{-5}$
Residual resistivity, Ω.m	$\rho := 1.68 \cdot 10^{-10}$	
Total constriction resistance, Ω	$R := \frac{\rho}{4 \cdot Ab}$	$R = 7.331 \times 10^{-7}$

Resistance Calculations - Splice Resistance

Splice Interface (1) – Copper Thimble and Sample

Residual resistivity of copper at 4.2K, Ω.m	$\rho cu := 1.48 \cdot 10^{-10}$	
Residual resistivity of solder at 4.2K, Ω.m	$\rho sr := 2 \cdot 10^{-9}$	
Outer diameter of copper ring, m	$\phi cu := 31.75 \cdot 10^{-3}$	
Outer diameter of solder, m	$\phi sr := 32.35 \cdot 10^{-3}$	
Thickness of copper ring, m	$tcu := 1 \cdot 10^{-3}$	
Thickness of solder, m	$tsr := 0.3 \cdot 10^{-3}$	
Copper resistance per unit length, Ω	$R := \frac{\rho cu \cdot 1}{3.14 \cdot \phi cu \cdot tcu}$	$R = 1.485 \times 10^{-6}$
Contact resistance across solder per unit length, Ω	$r := \frac{(\rho sr \cdot tsr)}{3.14 \cdot \phi sr \cdot 1}$	$r = 5.907 \times 10^{-12}$
Factor	$\alpha := \sqrt{\frac{R}{r}}$	$\alpha = 501.326$
Length of contact consider 2 turns, m	$L := 2 \cdot 10^{-3}$	Circumference (πd) x 2

Critical current, Amp	$It := 2000$	
Factor product	$F := \alpha \cdot L$	$F = 1.003$
Geometric factor	$f := \frac{\left(e^{F} + e^{-F}\right)}{\left(e^{F} - e^{-F}\right)}$	$f = 1.311$
Voltage, V	$VL := \left(It \cdot f \cdot \sqrt{r \cdot R}\right)$	$VL = 7.765 \times 10^{-6}$
Junction resistance, Ω	$Rj := \frac{VL}{It}$	$Rj = 3.882 \times 10^{-9}$

Splice Interface (1) – Copper Thimble and Sample

Residual resistivity of copper at 4.2K, Ω.m	$\rho cu := 1.48 \cdot 10^{-10}$	
Residual resistivity of solder at 4.2K, Ω.m	$\rho sr := 2 \cdot 10^{-9}$	
Outer diameter of copper ring, m	$\phi cu := 31.75 \cdot 10^{-3}$	
Outer diameter of solder, m	$\phi sr := 32.35 \cdot 10^{-3}$	
Thickness of extension piece, m	$tcu := 4.875 \cdot 10^{-3}$	
Thickness of solder, m	$tsr := 0.3 \cdot 10^{-3}$	
Copper resistance per unit length, Ω	$R := \frac{\rho cu \cdot 1}{3.14 \cdot \phi cu \cdot tcu}$	$R = 3.045 \times 10^{-7}$
Contact resistance across solder per unit length, Ω	$r := \frac{(\rho sr \cdot tsr)}{3.14 \cdot \phi sr \cdot 1}$	$r = 5.907 \times 10^{-12}$
Factor	$\alpha := \sqrt{\frac{R}{r}}$	$\alpha = 227.056$

Length of contact consider 2 turns, m	$L := 2 \cdot 10^{-3}$	circumference (πd) x 2
Critical current, Amp	$It := 2000$	
factor product	$F := \alpha \cdot L$	$F = 0.454$
Geometric factor	$f := \frac{\left(e^{F} + e^{-F}\right)}{\left(e^{F} - e^{-F}\right)}$	$f = 2.351$
Voltage, V	$VL := \left(It \cdot f \cdot \sqrt{r \cdot R}\right)$	$VL = 6.307 \times 10^{-6}$
Junction resistance, Ω	$Rj := \frac{VL}{It}$	$Rj = 3.154 \times 10^{-9}$

Appendix 4

Optimization of Current Leads – J. M. Lock's Method

From Lock's plot for copper, assuming the residual resistivity as 1.69e-8 Ω.cm (RRR=100)

The optimum geometric parameter is as follows:

Length of the conductor, cm $l := 100$

Current, amperes $I := 2000$

Conductor cross section, cm^2 $A := \frac{(l \cdot I)}{3.3 \cdot 10^5}$ $A = 0.606$

To calculate the diameter and the number of holes that can be cut from the leads

1. Outer Tube:

Outer diameter, cm $OD := 1.75 \cdot 2.54$ $OD = 4.445$

Inner diameter, cm $ID := 1.62 \cdot 2.54$ $ID = 4.115$

Wall thickness, cm $t := \frac{(OD - ID)}{2}$ $t = 0.165$

Cross sectional area of the tube, cm^2 $Ao := \left(\frac{3.14}{4}\right) \cdot \left(OD^2 - ID^2\right)$

$Ao = 2.219$

Area to be removed, cm^2 $Acut := Ao - A$ $Acut = 1.613$

Outer radius, cm $R1 := \frac{OD}{2}$ $R1 = 2.223$

Inner radius, cm $R2 := \frac{ID}{2}$ $R2 = 2.057$

Assume the diameter of the hole to be cut

Hole dia, cm $c := 0.8$

Outer radius of outer tube:

Distance from the chord to the center, cm $do := \sqrt{(R1)^2 - \left(\frac{c}{2}\right)^2}$ $do = 2.186$

Distance from top of curve to chord, cm $ho := R1 - do$ $ho = 0.036$

Area at top to be added, cm2 $Atop := \left(R1^2 \cdot acos\left(\frac{do}{R1}\right)\right) - do \cdot \sqrt{R1^2 - do^2}$

$Atop = 0.019$

Inner radius of outer tube:

Distance from the chord to the center, cm $di := \sqrt{(R2)^2 - \left(\frac{c}{2}\right)^2}$ $di = 2.018$

Distance from top pf curve to chord, cm $hi := R2 - di$ $hi = 0.039$

Area at bottom to be removed, cm2 $Abot := \left(R2^2 \cdot acos\left(\frac{di}{R2}\right)\right) - di \cdot \left(\sqrt{R2^2 - di^2}\right)$

$Abot = 0.021$

Area of rectangle, cm^2 $Arec := c \cdot t$ $Arec = 0.132$

Cross sectional area of 1 hole, cm^2 $Ahole := Arec + Atop - Abot$

$Ahole = 0.13$

Number of holes $n := 8$

Total CS area, cm^2 $At := Ahole \cdot n$ $At = 1.044$

Total CS to be cut, cm^2 $Acut = 1.613$

Ratio of volumes of outer tube with and without holes:

Length of the tube, cm $L := 129.424'$

Volume of tube, cm^3 $Vt := Ao \cdot L$ $Vt = 287.162$

Number of holes $nh := 55 \cdot 8$ $nh = 440$

Volume of holes, cm3 $Vh := \frac{3.14 \cdot \left(0.8^2\right) \cdot (t) \cdot nh}{4}$

$Vh = 36.496$

Volume of tube with holes, cm^3 $Vth := Vt - Vh$ $Vth = 250.666$

Ratio of volumes $Rv := \frac{Vt}{Vth}$ $Rv = 1.146$

2. Inner Tube:

Outer diameter, cm $OD := 1.25 \cdot 2.54$ $OD = 3.175$

Inner diameter, cm $ID := 1 \cdot 2.54$ $ID = 2.54$

Wall thickness, cm $t := \frac{(OD - ID)}{2}$ $t = 0.317$

Cross sectional area of the tube, cm^2 $Ao := \left(\frac{3.14}{4}\right) \cdot \left(OD^2 - ID^2\right)$

$Ao = 2.849$

Area to be removed, cm^2 $Acut := Ao - A$ $Acut = 2.243$

Outer radius, cm $R1 := \frac{OD}{2}$ $R1 = 1.587$

Inner radius, cm $R2 := \frac{ID}{2}$ $R2 = 1.27$

Assume the diameter of the hole to be cut

Hole dia, cm $c := 0.4$

Outer radius of outer tube:

Distance from the chord to the center, cm $do := \sqrt{(R1)^2 - \left(\frac{c}{2}\right)^2}$ $do = 1.575$

Distance from top of curve to chord, cm $ho := R1 - do$ $ho = 0.013$

Area at top to be added, cm^2

$$Atop := \left(R1^2 \cdot acos\left(\frac{do}{R1}\right)\right) - do \cdot \left(\sqrt{R1^2 - do^2}\right)$$

$$Atop = 3.376 \times 10^{-3}$$

Inner radius of outer tube:

Distance from the chord to the center, cm

$$di := \sqrt{(R2)^2 - \left(\frac{c}{2}\right)^2} \qquad di = 1.254$$

Distance from top of curve to chord, cm

$$hi := R2 - di \qquad hi = 0.016$$

Area at bottom to be removed, cm2

$$Abot := \left(R2^2 \cdot acos\left(\frac{di}{R2}\right)\right) - di \cdot \left(\sqrt{R2^2 - di^2}\right)$$

$$Abot = 4.231 \times 10^{-3}$$

Area of rectangle, cm^2

$$Arec := c \cdot t \qquad Arec = 0.127$$

Cross sectional area of 1 hole, cm^2

$$Ahole := Arec + Atop - Abot$$

$$Ahole = 0.126$$

Number of holes

$$n := 6$$

Total CS area, cm^2

$$At := Ahole \cdot n \qquad At = 0.757$$

Total CS to be cut, cm^2

$$Acut = 2.243$$

Ratio of volumes of outer tube with and without holes:

Length of the tube, cm	$L := 138.437$	
Volume of tube, cm^3	$Vt := Ao \cdot L$	$Vt = 394.378$
Number of holes	$nh := 75 \cdot 6$	$nh = 450$
Volume of holes, cm3	$Vh := \frac{3.14 \cdot \left(0.4^2\right) \cdot (t) \cdot nh}{4}$	
	$Vh = 17.945$	
Volume of tube with holes, cm^3	$Vth := Vt - Vh$	$Vth = 376.433$
Ratio of volumes	$Rv := \frac{Vt}{Vth}$	$Rv = 1.048$

Appendix 5

Shear Stress Calculations

Outer Current Tube:

Length of the outer current tube, mm $L := 50.95 \cdot 25.4$ $L = 1.294 \times 10^3$

Outer Diameter of the tube, mm $D := 1.75 \cdot 25.4$ $D = 44.45$

Inner diameter of the tube, mm $d := 1.625 \cdot 25.4$ $d = 41.275$

Polar moment of inertia of the cross section accounting for only 50% of section, mm^4 $Ip := \frac{0.5 \cdot 3.14}{32} \cdot \left(D^4 - d^4\right)$

$Ip = 4.913 \times 10^4$

Shear modulus of copper, MPa $G := 4500($

Total torque applied, N.mm $T := 3000($

Angular of twist, rad $\phi := \frac{(T \cdot L)}{G \cdot Ip}$ $\phi = 0.018$

Angular of twist, deg $\phi d := \phi \cdot \frac{180}{3.14}$ $\phi d = 1.007$

Shear stresses

Shear stress in the probe, MPa $\tau max := \frac{T \cdot D}{2 \cdot Ip}$ $\tau max = 13.57$

Shear yield of copper, MPa $Ssy := 0.4 \cdot 22($ $Ssy = 88$

Factor of safety $n := \frac{Ssy}{\tau max}$ $n = 6.485$

The design is within the safe limits

Shear stress in dowel pins connecting transition piece and spring

Diameter of the Torque circle, mm	$D := 26.875$	$D = 26.875$
Torque applied on tube, N.mm	$T := 3000$	
Shear force due to torque on pins, N	$F := \frac{T}{D}$	$F = 1.116 \times 10^3$
Dia of dowel pins, mm	$d := 3$	
Area of cross section of pins, mm^2	$A := \frac{3.14 \cdot d^2}{4}$	$A = 7.065$
Number of shear areas	$n := 1$	
Shear stress on pins, MPa	$\tau := \frac{F}{n \cdot A}$	$\tau = 158.001$
Shear stress if 6 pins used, MPa	$\tau n := \frac{\tau}{6}$	$\tau n = 26.334$

Tensile Yield strength of 18-8 (304SS) is ~ 200 MPa

Shear yield strength of structural steel, MPa	$Ssy := 0.4 \cdot 200$	$Ssy = 80$
Factor of safety	$f := \frac{Ssy}{\tau n}$	$f = 3.038$

Thus the design is within safe operating limits.

Shear stress in screws for bottom copper thimble

Diameter of the Torque circle, mm	$D := 23.875$	$D = 23.875$
Torque applied on tube, N.mm	$T := 30000$	
Shear force due to torque on pins, N	$F := \frac{T}{D}$	$F = 1.257 \times 10^3$
Minor dia of M2.5 screw, mm	$d := 1.938$	
Area of cross section of pins, mm^2	$A := \frac{3.14 d^2}{4}$	$A = 2.948$
Number of shear areas	$n := 1$	
Shear stress on screws, MPa	$\tau := \frac{F}{n \cdot A}$	$\tau = 426.187$
Shear stress if 10 screws used, MPa	$\tau n := \frac{\tau}{10}$	$\tau n = 42.619$

Tensile Yield strength of 18-8 (304SS) is ~ 200 MPa

Shear yield strength of structural steel, MPa	$Ssy := 0.4 \cdot 200$	$Ssy = 80$
Factor of safety	$f := \frac{Ssy}{\tau n}$	$f = 1.877$

Thus the design is within safe operating limits.

Shear stress in screws for outer extension tube

Diameter of the Torque circle, mm	$D := 1.625 \cdot 25.4$	$D = 41.275$
Torque applied on tube, N.mm	$T := 3000($	
Shear force due to torque on pins, N	$F := \frac{T}{D}$	$F = 726.832$
Minor dia of M3 screw, mm	$d := 2.387$	
Area of cross section of pins, mm^2	$A := \frac{3.14 \cdot d^2}{4}$	$A = 4.473$
Number of shear areas	$n := 1$	
Shear stress on screws, MPa	$\tau := \frac{F}{n \cdot A}$	$\tau = 162.502$
Shear stress if 6 screws used, MPa	$\tau n := \frac{\tau}{12}$	$\tau n = 13.542$

Tensile Yield strength of 18-8 (304SS) is ~ 200 MPa

Shear yield strength of structural steel, MPa	$Ssy := 0.4 \cdot 200$	$Ssy = 80$
Factor of safety	$f := \frac{Ssy}{\tau n}$	$f = 5.908$

Thus the design is within safe operating limits.